Measurement Report: Abundance and fractional solubilities of aerosol metals in urban Hong Kong: Insights into factors that control aerosol metal dissolution in an urban site in South China

Junwei Yang,[1] Lan Ma,[1] Xiao He,[2] Wing Chi Au,[1] Yanhao Miao,[1] Wen-Xiong Wang,[1,3] Theodora Nah[1,3]*

[1]*School of Energy and Environment, City University of Hong Kong, Hong Kong SAR, China*

[2]*College of Chemistry and Environmental Engineering, Shenzhen University, Shenzhen 518060, China*

[3]*State Key Laboratory of Marine Pollution, City University of Hong Kong, Hong Kong SAR, China*

** To whom correspondence should be addressed: Theodora Nah (Email: theodora.nah@cityu.edu.hk)*

Abstract

Water-soluble metals are known to produce greater adverse human health outcomes than their water-insoluble forms. Although the concentrations of water-soluble aerosol metals are usually limited by atmospheric processes that convert water-insoluble metals to water-soluble forms, factors that control the solubilities of aerosol metals in different environments remain poorly understood. In this study, we investigated the abundance and fractional solubilities of different metals in size-fractionated aerosols collected at an urban site in Hong Kong, and identified the factors that modulated metal solubilities in fine aerosols. The concentrations of total and water-soluble metals in fine and coarse aerosols were the highest during the winter and spring seasons due to the long-range transport of air masses by northly prevailing winds from emission sources located in continental areas north of Hong Kong. The study-averaged metal fractional solubilities spanned a wide range for both fine (7.8 % to 71.2 %) and coarse (0.4 % to 47.9 %) aerosols, but higher fractional solubilities were typically observed for fine aerosols. Sulfate was found to be strongly associated with both the concentrations of water-soluble Cr, Fe, Co, Cu, Pb, and Mn and their fractional solubilities in fine aerosols, which implied that sulfate-driven acid processing likely played an important role in the dissolution of the water-insoluble forms for these six metals. Further analyses revealed that these strong associations were due to sulfate providing both the acidic environment and liquid water reaction medium needed for the acid dissolution process. Thus, the variability in the concentrations of water-soluble Cr, Fe, Co, Cu, Pb, and Mn and their fractional solubilities were driven by both the aerosol acidity levels and liquid water concentrations, which in turn were controlled by sulfate. These results highlight the roles that sulfate plays in the acid dissolution of metals in fine aerosols in Hong Kong. Our findings will likely also apply to other urban areas in South China, where sulfate is the dominant acidic and hygroscopic component in fine aerosols.

Deleted: 8.8

Deleted: 70.3

Deleted: 1.4

Deleted: 54.3

1. Introduction

Chronic exposures to atmospheric aerosols, especially those in the fine mode ($PM_{2.5}$, aerosols with aerodynamic diameter ≤ 2.5 μm), have been linked to a myriad of deleterious effects on human health, including morbidity and excessive deaths through respiratory and cardiovascular diseases (Brook et al., 2010; Cohen et al., 2017). Some of the aerosol chemical species cause majority of the adverse human health outcomes even though they comprise a small fraction of the overall aerosol mass (Phalen, 2004; Lippmann, 2014). Metals are ubiquitous chemical species that contribute significantly to airborne aerosol toxicity even though they are typically present in aerosols in trace quantities (Costa and Dreher, 1997a; Frampton et al., 1999; Ye et al., 2018; Zhao et al., 2021). Natural sources, especially mineral dust and sea spray, dominate the global sources of aerosol metals (Nriagu, 1989; Garrett, 2000; Deguillaume et al., 2005; Mahowald et al., 2018). However, anthropogenic sources such as industrial activities and vehicular traffic contribute substantial quantities of aerosol metals in urban environments (Garg et al., 2000; Adachi and Tainosho, 2004; Deguillaume et al., 2005; Lough et al., 2005; Birmili et al., 2006; Lee et al., 2007; Cheng et al., 2009; Li et al., 2013; Jiang et al., 2015; Mahowald et al., 2018).

Metals exist in aerosols in water-insoluble and water-soluble forms. Compared to their water-insoluble forms, water-soluble metals have higher bioavailability, which reportedly allows them to produce adverse human health outcomes (Costa and Dreher, 1997b; Heal et al., 2009; Fang et al., 2015; Gao et al., 2020a; He et al., 2021). Some water-soluble transition metal ions (e.g., Fe(II), Fe(III), Cu(I), Cu(II)) are redox-active species and serve as catalysts in reaction cycles (e.g., Fenton-like reactions) to enhance the *in vivo* production of reactive oxygen species (ROS) (e.g., ·OH, HO_2·, H_2O_2), which subsequently induce the physiological oxidative stress and inflammation involved in a variety of chronic and acute diseases (Bresgen and Eckl, 2015; Lakey et al., 2016; Bates et al., 2019). A recent epidemiologic study reported that water-soluble Fe concentrations in $PM_{2.5}$ showed strong correlations with cardiovascular-related emergency department visits in Atlanta (Ye et al., 2018). Less abundant water-soluble aerosol metals such as Cr and Pb are also known to exhibit both carcinogenic and noncarcinogenic risks to adults and children despite their small quantities (He et al., 2021).

Deleted: W

Deleted: and usually have been reported to

Deleted:

Deleted: greater

Deleted: than their water-insoluble forms

Deleted: ·

Water-soluble metals also play important roles in ocean biogeochemistry and atmospheric processes. Atmospheric aerosol deposition is an important source of bioavailable dissolved metals in open oceans. The dissolved metals serve as nutrients, and in some cases toxins, for various aquatic species (De Baar et al., 2005; Boyd et al., 2007; Paytan et al., 2009; Jordi et al., 2012). Some transition metal ions such as Fe(III) and Mn(II) ions can facilitate the formation and aging of organic aerosols (Chu et al., 2013; Al-Abadleh, 2015; Slikboer et al., 2015; Chu et al., 2017; Al-Abadleh, 2021), The coupled redox cycling of Cu(I)/Cu(II) and Fe(II)/Fe(III) ions in aerosols has been proposed to be an important mechanism for the uptake of gas-phase HO_2 in aqueous aerosols, which has important implications for the tropospheric OH radical and O_3 budget (Mao et al., 2013; Mao et al., 2017). Mn(II)-catalyzed oxidation of SO_2 on aqueous aerosol surfaces reportedly contributes more than 90 % of the sulfate production during wintertime haze events in China (Wang et al., 2021).

Aerosol metals are primarily emitted into the atmosphere in water-insoluble forms (Nriagu, 1989). While water-soluble aerosol metals can be emitted directly into the atmosphere (Fang et al., 2015), the concentrations of water-soluble aerosol metals are likely limited by atmospheric processes that convert the water-insoluble metal forms to water-soluble forms (Mahowald et al., 2018). Given the important roles that water-soluble aerosol metals play in adverse human health outcomes and atmospheric processes, it is necessary to understand the factors that modulate the atmospheric processing, and hence the solubility, of aerosol metals. Aerosol Fe dissolution has been the focus of most previous studies. A wide range (<1 % to 98 %) of fractional solubilities (ratio of the water-soluble metal mass concentration to the total metal mass concentration) has been reported for Fe in atmospheric aerosols (Mahowald et al., 2018). Anthropogenic-influenced aerosols generally have higher Fe solubility than fresh mineral dust (Sedwick et al., 2007; Schroth et al., 2009; Oakes et al., 2012). However, Fe solubility varies substantially in aerosols in different urban environments with high levels of anthropogenic activities (e.g., 1 % to 12 % in four cities in East China (Zhu et al., 2020) vs. around 20 % to 50 % in Hong Kong, South China (Jiang et al., 2014; Jiang et al., 2015). Although there are a number of atmospheric processes that can influence aerosol metal solubilities, acid processing and the formation of stable Fe-organic complexes are two key

Deleted: many

chemical processes known to enhance aerosol Fe dissolution (Deguillaume et al., 2005; Ingall et al., 2018; Tao and Murphy, 2019; Giorio et al., 2022). At present, it remains difficult to explain the variability of aerosol Fe solubility in urban environments since the extent to which aerosol Fe dissolution is controlled by factors such as aerosol acidity and/or the presence of organic ligands (e.g., oxalate) in different urban environments is still not well understood. Even less is known about the factors that control the solubilities of other aerosol metals beyond Fe.

Hong Kong is a highly developed, densely populated city in the Guangdong-Hong Kong-Macau Great Bay Area (GBA) urban agglomeration, which is a large business and economic hub located in the southern part of China. While there have been some studies on the fractional solubilities of various aerosol metals in Hong Kong (Jiang et al., 2014; Jiang et al., 2015), to the best of our knowledge, there has not been a study that has investigated the factors that control the solubilities of aerosol metals in Hong Kong. In this study, we investigated the abundance and fractional solubilities of ten metals (Fe, Cu, Al, V, Cr, Mn, Co, Ni, Cd, and Pb) in aerosols at an urban site in Hong Kong. Our main goal is to identify the key factors that control the solubilities of metals in fine aerosols since they are believed to exert higher toxicity than coarse aerosols due to their small sizes. We focus primarily on aerosol metal dissolution through the acid processing and/or metal-organic complexation mechanisms. Hence, other aerosol species were also measured for comparisons to total and water-soluble metals. The measured aerosol inorganic ion composition was used as inputs for a thermodynamic model to determine the aerosol acidity levels, liquid water concentrations, and pH.

2. Methods

2.1. Ambient sampling

The sampling campaign took place at ground level next to a road in Kowloon Tong (22.3367° N, 114.1724° E). Kowloon Tong is located in the southern side of Hong Kong, and it is primarily a residential and commercial district which is close to Mongkok, one of the busiest commercial and most densely populated areas in Hong Kong with high density traffic flow. Weekly size-fractionated aerosol samples were collected on 7 March 2021 to 4 April 2021 (spring season), 23 to 30 June 2021 and 7 to 14 July 2021 (summer season), 13 September

2021 to 11 October 2021 (fall season), and 15 December 2021 to 26 January 2022 (winter season). Back-trajectories calculations calculated by the Hybrid Split-Particle Lagrangian Integrated Trajectory (HYSPLIT) model using meteorological data from NCEP/NCAR Reanalysis (2.5° latitude-longitude grid) showed that the sampling site was under the influence of continental and marine air masses during the sampling periods, though the contributions of these air masses varied with the season (Figure S1).

An eleven stage Micro-Orifice Uniform Deposit Impactor (MOUDI) (Model 110, MSP Corp., USA) was used to collect and divide aerosols into different aerosol size bins under ambient conditions. Aerosols were collected on prebaked 47 mm diameter quartz filters (Tissuquartz 2500QAT-UP, Pall Corp., USA). The nominal cut points for the MOUDI eleven impactor stages were 0.056 μm, 0.1 μm, 0.18 μm, 0.32 μm, 0.56 μm, 1.0 μm, 1.8 μm, 3.2 μm, 5.6 μm, 10 μm, and 18 μm. In the discussion below, for simplicity, we refer to aerosols collected on impactor stages with nominal cut points 0.056 μm, 0.1 μm, 0.18 μm, 0.32 μm, 0.56 μm, 1.0 μm, and 1.8 μm as "fine aerosols", while aerosols collected on impactor stages with nominal cut points 3.2 μm, 5.6 μm, 10 μm, and 18 μm were referred to as "coarse aerosols". Aerosols were collected continuously for seven days (i.e., 24 hours × 7 days). This resulted in a total of four, two, four, and six weekly sets of aerosol filter samples collected during the spring, summer, fall, and winter seasons, respectively. After collection, the aerosol filter samples were immediately extracted for chemical analysis.

Thermodynamic model calculations used to determine the aerosol acidity levels, liquid water concentrations, and pH (Section 2.3) require gas-phase NH_3 concentrations, ambient temperature and relative humidity (RH) as model inputs. Hence, weekly NH_3 measurements were performed during each sampling period using four passive sampling devices (PSDs) and pre-coated collection pads (PS-100 and PS-154, Ogawa & Co., Pompano Beach, FL), except from 7 to 28 March 2021. The exposed PSD collection pads were extracted in purified deionized water (18.2 MΩ-cm) using the protocol recommended by the manufacturer. These aqueous extracts were subsequently analyzed by ion chromatography (Section 2.2) to determine the average NH_3 concentration during the sampling period. A Vantage Vue Weather Station (Model 6250, Davis Instruments, USA) was used to measure ambient temperature and

RH during each sampling period.

2.2. Chemical analysis

Each aerosol filter sample was cut into four equal pieces for chemical analysis of different chemical components. One of the four pieces was extracted in purified deionized water via sonication (1 hour), followed by high speed vortexing at 3000 rpm (15 minutes). The resulting aqueous extract was filtered using 0.22 μm pore size nylon filters (Jinteng Instrument Co., Tianjin, China) before it was analyzed by a Total Organic Carbon (TOC) analyzer (TOC-VCSH, Shimadzu, Japan) to determine the concentration of water-soluble organic carbon (WSOC). The TOC analyzer has a limit of detection (LOD) of 0.5 mg L^{-1}. The second filter piece was similarly extracted in purified deionized water via sonication (1 hour) and high speed vortexing at 3000 rpm (15 minutes), and filtered using 0.22 μm pore size nylon filters before it was analyzed by an ion chromatography (IC) system (Dionex ICS-1100, ThermoFisher Scientific, USA) using an isocratic method to determine the concentrations of water-soluble anions (NO_3^-, SO_4^{2-}, Cl^-, and $C_2O_4^{2-}$) and cations (NH_4^+, Na^+, K^+, Ca^{2+}, and Mg^{2+}). Anion separation was achieved using a 4 × 250 mm anion exchange column (Dionex IonPac AS18, ThermoFisher Scientific, USA) equipped with a 4 × 50 mm guard column (Dionex IonPac AG18, ThermoFisher Scientific, USA). Cation separation was achieved using a 4 × 250 mm cation exchange column (Dionex IonPac CS12A, ThermoFisher Scientific, USA) equipped with a 4 × 50 mm guard column (Dionex IonPac CG12A, ThermoFisher Scientific, USA). 16 mM potassium hydroxide and 31 mM methanesulfonic acid were used as eluents at a flowrate of 1.0 mL min^{-1} for the anion and cation separations, respectively. The cation IC method was also used to analyze the aqueous extracts from the exposed PSD collection pads to determine the average NH_3 concentration during each sampling week. The LODs for the cation IC method were 0.025 mg L^{-1} for NH_4^+, Na^+, and Mg^{2+}, and 0.025 mg L^{-1} for K^+ and Ca^{2+}. The LODs for the anion IC method were 0.125 mg L^{-1} for NO_3^-, SO_4^{2-}, and $C_2O_4^{2-}$, and 0.025 mg L^{-1} for Cl^-.

The remaining two filter pieces were used for metal analysis. One filter piece was extracted with purified deionized water in metal-free centrifuge tubes via sonication (1 hour), followed by high speed vortexing at 3000 rpm (15 minutes). The resulting aqueous extract was

Deleted: , and then

filtered using 0.22 µm pore size nylon filters, and acidified with 2 % HNO_3 prior to storage at 4 °C before chemical analysis of water-soluble metals. The filterable metal fraction in the water extracts, defined in this study as water-soluble metals, will include all dissolved metal forms and any colloidal particles with diameters smaller than 0.22 µm. This assumes that all colloidal particles with diameters smaller than 0.22 µm can penetrate through the syringe filter, and that the syringe filter's retention efficiency of particles with diameters larger than 0.22 µm is 100 %. The exact sizes and distribution of metal colloidal particles in the filterable metal fraction in water extracts in this study are not known. However, Yang et al. (2021) recently reported that around 84% of Fe and Cu colloidal particles that penetrated through 0.45 µm syringe filters had nominal diameters smaller than 4 nm. The remaining 16% of Fe and Cu colloidal particles had nominal diameters between 4 nm and 0.45 µm, and they may be in water-insoluble forms (e.g., Fe and Cu oxides) so they may not be "true" water-soluble species. Hence, analogous to observations made by Yang et al (2021), it is possible that the filterable metal fractions in water extracts in this study contain some metals in water-insoluble forms with diameters smaller than 0.22 µm that penetrated through the 0.22 µm pore size filters. The last filter piece was extracted via acid digestion for chemical analysis of total metals. The acid digestion protocol we employed was adapted from published protocols (Jiang et al., 2014; Jiang et al., 2015). The filter piece was extracted in an acid digestion matrix (16 N HNO_3 and 12 N HCl at a 3:1 volume ratio) placed in a glass microwave vial using a microwave synthesizer (Initiator+, Biotage, Sweden). The microwave synthesizer's digestion temperature was ramped up to 150 °C, and then held for 15 min. This was followed by cooling and ventilation for 30 minutes. An evaporation and recovery treatment was next performed to remove Cl^- from the matrix to reduce its interference during chemical analysis. The digestion solution was heated to 200 °C on a hotplate. Once the solution was observed to be almost dry, 16 N HNO_3 was added to the solution. When the solution was observed to be almost dry the second time, 2 % HNO_3 was added to the solution. The resulting solution was filtered using 0.22 µm pore size nylon filters, and then stored at 4 °C before chemical analysis of total metals. A standard reference material of San Joaquin soil (SRM 2709a, NIST) was digested and analyzed using the same protocols to evaluate the metal recoveries. Recoveries of 59.4 % for Cr, 67.0 % for Al, 93.7 % for Fe,

93.6 % for Ni, 100.2 % for Co, 98.6 % for Pb, 95.8 % for Cu, 99.6 % for Mn, 70.5 % for V, and 94.3 % for Cd were observed.

The concentrations of ten water-soluble and total metals (^{27}Al, ^{51}V, ^{52}Cr, ^{55}Mn, ^{57}Fe, ^{59}Co, ^{60}Ni, ^{65}Cu, ^{111}Cd, and ^{208}Pb) were determined by an Inductively Coupled Plasma–Mass Spectrometry (ICP–MS) instrument (NexION 1000, PerkinElmer Inc., USA). The following parameters were used for the ICP-MS instrument: 0.98 L min^{-1} nebulizer gas flow, 1.2 L min^{-1} auxiliary gas flow, 15 L min^{-1} plasma gas flow, 5 mL min^{-1} He gas flow, 1600 W RF power, 35 rpm nebulizer pump rate, and 35 rpm sample pump rate. A multi-elemental calibration standard (IV-STOCK-13, Inorganic Ventures, USA) was used to quantify the ten water-soluble and total metals. An internal standard solution of ^{115}In (10 µg L^{-1}) was added to all samples and standards to monitor analytical drift. The LODs for ^{27}Al, ^{51}V, ^{52}Cr, ^{55}Mn, ^{57}Fe, ^{59}Co, ^{60}Ni, ^{65}Cu, ^{111}Cd, and ^{208}Pb were 87, 0.8, 2.8, 1.6, 277, 0.7, 4.6, 6.7, 1, and 0.4 ng L^{-1}, respectively. To identify the major sources of the aerosol metals, source apportionment was performed with positive matrix factorization (PMF) (Paatero and Tapper, 1994; Paatero, 1997) using the aerosol chemical components measured by the ICP-MS and IC. Details of the PMF method used can be found in Section S1 (SI).

Deleted: ng L^{-1}

Deleted: ng L^{-1}

Deleted: ng L^{-1}

Deleted: ng L^{-1}

Deleted: ng L^{-1}

Deleted: ng L^{-1}

Deleted: ng L^{-1}

Deleted: ng L^{-1}

2.3. Thermodynamic modeling

The thermodynamic model ISORROPIA-II was used to determine aerosol acidity levels, liquid water concentrations, and pH (Fountoukis and Nenes, 2007). Similar to the methodology employed by Fang et al. (2017), we ran ISORROPIA-II for each of the MOUDI impactor stages that collected fine aerosols. The measured water-soluble NH_4^+, SO_4^{2-}, NO_3^-, Cl^-, Na^+, Ca^{2+}, K^+, and Mg^{2+} ions for the aerosols collected on the MOUDI impactor stage, gas-phase NH_3, ambient temperature and RH were used as model inputs. Since gas-phase NH_3 measurements were not available from 7 to 28 March 2021, we used NH_3 measurements from 28 March to 4 April 2021 as model inputs for the spring calculations. The measured NH_3 concentrations during the study ranged from 3.60 µg m^{-3} to 8.18 µg m^{-3}, with a study-averaged concentration of 5.01 ± 1.25 µg m^{-3}. ISORROPIA-II was run in "forward" mode and under the assumption that the aerosols existed in a "metastable" equilibrium state (i.e., the aerosols only existed in

liquid form). These calculations assumed that the aerosols were in thermodynamic equilibrium with the gas phase. While fine aerosols satisfy this equilibrium condition, equilibrium between the gas and aerosol phases of coarse aerosols cannot be achieved due to kinetic limitations (Fountoukis et al., 2009). Thus, aerosol pH values were not calculated for coarse aerosols.

Fine aerosol pH values were calculated based on the molal definition (Pye et al., 2020):

$$pH = -\log_{10} \gamma_{H^+} H^+_{aq} = -\log_{10} \frac{1000 H^+_{air}}{W_i + W_o} \cong -\log_{10} \frac{1000 H^+_{air}}{W_i} \quad (1)$$

where γ_{H^+} is the hydronium ion activity coefficient, H^+_{aq} is the hydronium ion concentration within the ambient aerosol liquid water (mol L^{-1}), H^+_{air} is the hydronium ion concentration per volume of air (µg m^{-3}), and W_i and W_o are the aerosol liquid water concentrations (µg m^{-3}) associated with inorganic and organic species, respectively. H^+_{air} and W_i are the outputs provided by the ISORROPIA-II model, which assumes that γ_{H^+} is equals to unity. W_o can be estimated from the WSOC measurements using the approach described in Section S2 (SI). WSOC concentrations in the size-fractionated aerosols ranged from 0 to 4.6 µg m^{-3}. The inclusion of W_o into calculations did not impact aerosol pH significantly (Figure S2). Thus, only aerosol pH values calculated using W_i will be reported here. Similar to Fang et al. (2017), lower pH values were typically calculated for aerosols collected on MOUDI impactor stages with smaller nominal cut points (i.e., these aerosols had smaller aerodynamic aerosol diameters) due to the higher mass concentrations of sulfate in these smaller aerosols. The fine aerosols were mostly acidic, with about 74 % of the calculated pH values lying between 2 and 4.

3. Results and discussion

3.1. Total metals

Figure 1 shows the seasonal average mass concentrations of the ten measured total metals in size-fractionated aerosols. The size distributions of five of the metals (Al, Fe, Mn, V, and Cd) consistently exhibited a single mode. The modes for Mn, V, and Cd were predominantly found in the fine mode, while the modes for Fe and Al were predominantly found in the coarse aerosol mode. Figure 2a shows the seasonal average concentrations of the ten measured total metals in fine and coarse aerosols. For most of the metals, higher mass

concentrations were measured during the winter and/or spring seasons. This could be attributed to the long-range transport of polluted air masses by northly prevailing winds from emission sources located in continental areas north of Hong Kong (Figure S1). The metals could be arranged in the following order based on their abundances: Fe > Al > Cu > Co > Mn > Pb > Cr > Ni > V > Cd. This order of abundance was the same for both fine and coarse aerosols.

The mass concentrations of the two most abundant metals, Fe and Al, were usually higher than 10 ng m^{-3} in both fine and coarse aerosols. Fe, Al, and Cu had substantially higher mass concentrations in coarse aerosols than in fine aerosols. The positive correlations between the mass concentrations of Al with the mass concentrations of Fe and Cu were the strongest among the nine metals (R = 0.62 and R = 0.52, respectively) and statistically significant (Figure S3), which could be explained by large mass concentrations of Al, Fe, and Cu originating from similar sources. These three metals are known to originate mainly from dust sources (e.g., mineral dust and road dust) (Hopke et al., 1980; Garg et al., 2000; Adachi and Tainosho, 2004; Lough et al., 2005; Chow et al., 2022). This is consistent with results from our PMF source apportionment analysis, which showed that the "dust" factor had large mass contributions from Al, Fe, and Cu (Figures S4 and S5). Mn, Ni, V, and Cd had higher mass concentrations in fine aerosols than in coarse aerosols. These four metals are known to be consistently found in aerosols from anthropogenic sources such as vehicle and ship emissions, combustion and industrial processes (Chow et al., 2022). Pb, Cr, and Co had mostly similar concentrations in the fine and coarse aerosols. Interestingly, the mass concentrations of Mn and Cr were positively correlated with the mass concentration of Al (R = 0.42 and R = 0.33, respectively), and these correlations were statistically significant (Figure S3). Our PMF analysis apportioned Al to two factors, "dust" and "industrial factor 1", though the Al contribution to "industrial factor 1" was substantially smaller compared to "dust" (Figures S4 and S5). The "dust" factor had a significant Mn contribution, which could explain the strong correlation between the mass concentrations of Al and Mn. Cr was apportioned primarily to "industrial factor 1", which could explain the strong correlation between the mass concentrations of Al and Cr. The mass concentrations of Ni, V, Cd, Pb, and Co showed weak correlations with the mass concentration of Al (Figure S3).

Deleted: Fe > Al > Cu > Mn > Pb > Ni > Cr > V > Co > Cd

Deleted: Figure S3 shows the correlation between mass concentration of total Al and other metals for both fine and coarse aerosols. The correlations between Al with Fe and Cu are statistically significant, and Fe and Cu have the highest correlation coefficient, which indicates Al, Fe, Cu likely come from similar sources

Deleted: In contrast,

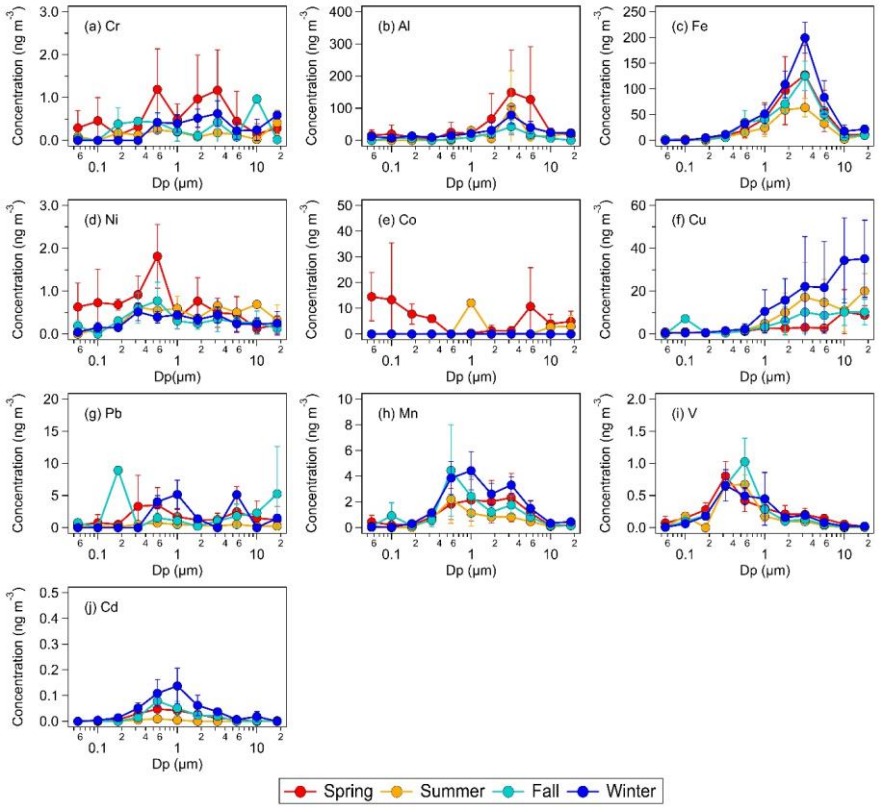

Figure 1: Seasonal average concentrations of total elemental metals in size-fractionated aerosols sampled by the MOUDI with the following nominal cut points (Dp): 0.056 μm (size fraction 1), 0.1 μm (size fraction 2), 0.18 μm (size fraction 3), 0.32 μm (size fraction 4), 0.56 μm (size fraction 5), 1.0 μm (size fraction 6), 1.8 μm (size fraction 7), 3.2 μm (size fraction 8), 5.6 μm (size fraction 9), 10 μm (size fraction 10), and 18 μm (size fraction 11). The error bars represent one standard deviation of the seasonal average value.

Deleted: concentrations in the fine and coarse aerosols. ¶

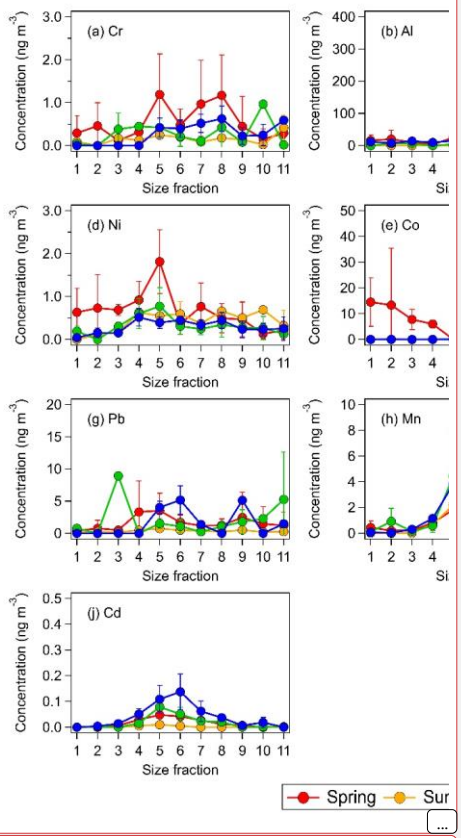

Formatted: Justified, Add space between paragraphs of the same style

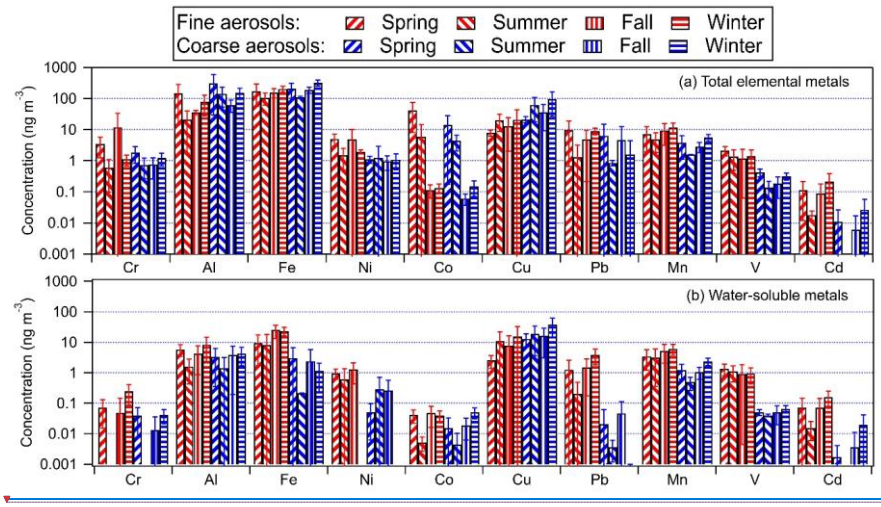

Figure 2: Seasonal average mass concentrations of (a) total metals and (b) water-soluble metals in fine (red) and coarse (blue) aerosols. The error bars represent one standard deviation. The y axes are on logarithm scales.

Jiang et al. (2015) previously measured the mass concentrations of various total metals in $PM_{2.5}$ and $PM_{2.5\text{-}10}$ in Kowloon Tong. The authors carried out their measurements from 12 November 2012 to 10 December 2012 (winter) and from 8 April 2013 to 13 May 2013 (spring/summer). To gain some insights into how the aerosol metal concentrations at this urban site have changed since 2012/2013, we compared the average mass concentrations of total metals in fine and coarse aerosols measured in this study to those measured by Jiang et al. (2015). As shown in Table S1, lower mass concentrations were measured in fine (21 % to 93 % lower) and coarse (0.5 % to 92 % lower) aerosols for most of the metals in this study. While the lower aerosol metal mass concentrations could be partly attributed to lower levels of anthropogenic activities in 2021/2022 due to COVID-19, it is likely that the implementation of numerous local and regional air pollution policies to reduce industrial and transport-related emissions over the last decade contributed largely to this decrease. For instance, industrial upgrades resulting from the implementation of the "double transfer" policy (industry and labor transfer away from primary industries) in Guangdong likely caused the decline in the mass concentrations of metals that are typically associated with industrial activities such as Cu and

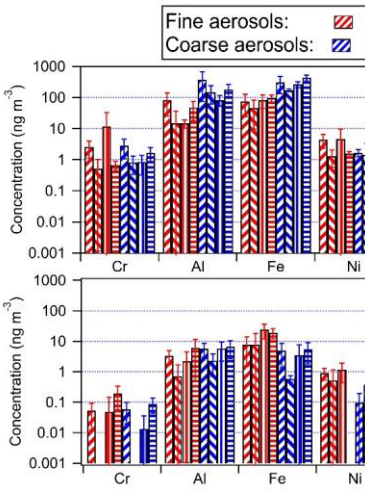

Deleted:

Deleted:

Deleted: yellow

Deleted: 30

Deleted: 94

Deleted: 7

Deleted: 80

Mn (Zhong et al., 2013; Chow et al., 2022). In addition, government policies driving the switch to cleaner fuels for energy generation and transport in Hong Kong and the GBA likely caused the decline in the mass concentrations of metals such as Pb, Ni, V, and Fe. Interestingly, higher mass concentrations were measured for Fe and Cu in coarse aerosols in this study compared to those measured by Jiang et al. (2015). Fe and Cu in coarse aerosols have previously been linked to resuspended road dust from brake and tire wear (Garg et al., 2000; Adachi and Tainosho, 2004; Lough et al., 2005). Based on publicly available government data (www.td.gov.hk), the number of registered motor vehicles in Hong Kong has increased by about 34 % over the last decade. It is possible that the higher Fe and Cu mass concentrations in coarse aerosols in this study were due to increased contributions from road dust as a result of increased vehicle fleet size at the urban site.

A PMF source apportionment analysis was performed to determine the major sources of aerosol metals measured in this study (Section S1). A five-factor solution was selected since it gave the most reasonable factor profiles and had high stability. The five factors were broadly classified as "sea salt", "dust", "ship emissions", "industrial factor 1", and "industrial factor 2" based on the tracer species with the highest mass loadings in each factor (Figure S4). A discussion on how these five factors were classified can be found in Section S1. Figure S5 shows the seasonal mass contributions of each source to each metal species in coarse and fine aerosols. Metals with large fractions in the dust and sea salt source factor profiles generally had higher mass concentrations in coarse aerosols. Conversely, metals with large fractions in the ship emissions and industrial source factor profiles generally had higher mass concentrations in fine aerosols. Higher mass contributions were usually observed in the winter and/or spring seasons, which could be attributed to the long-range transport of polluted air masses by northly prevailing winds from emission sources located in continental areas north of Hong Kong (Figure S1).

Deleted: identified

Deleted: S3

Deleted: S4

3.2. Water-soluble metals

Figure 3 shows the seasonal average mass concentrations of water-soluble metals in size-fractionated aerosols. The size distribution of six of the water-soluble metals (Cr, Fe, Pb,

Mn, V, and Cd) mostly exhibited a single mode, all of which were found in the fine aerosol mode. Fe, Mn, V, and Cd exhibited a single mode for both their total and water-soluble components (Figures 1 and 3). Of these four metals, only the modes of total and water-soluble Fe showed obvious differences, with total Fe exhibiting a mode at around 3.2 μm (size fraction 8) and water-soluble Fe exhibiting a mode at around 0.56 μm to 1.0 μm (size fractions 5 to 6). The modes of total and water-soluble Cu also showed obvious differences. While the mode of total Cu was at ≥18 μm (Figure 1f), the modes of water-soluble Cu were found at substantially small aerosol sizes (Figure 3f).

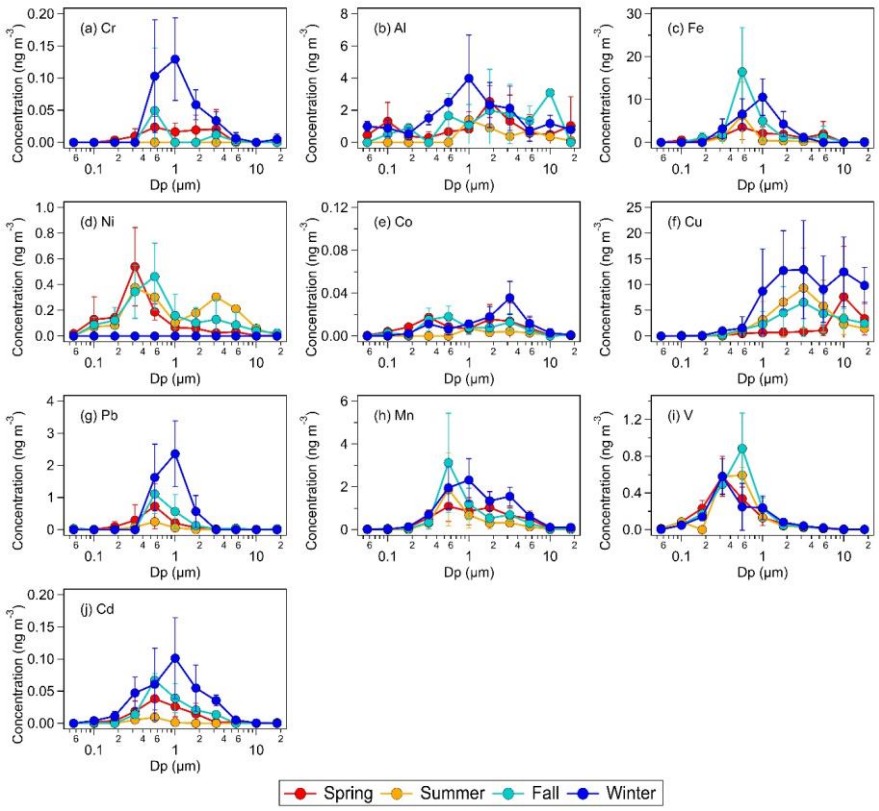

Figure 3: Seasonal average concentrations of water-soluble metals in size-fractionated aerosols sampled by the MOUDI with the following nominal cut points (Dp): 0.056 μm (size fraction 1), 0.1 μm (size fraction 2), 0.18 μm (size fraction 3), 0.32 μm (size fraction 4), 0.56 μm (size

Deleted: S

Deleted: smaller aerosol sizes (Figure 3f).¶

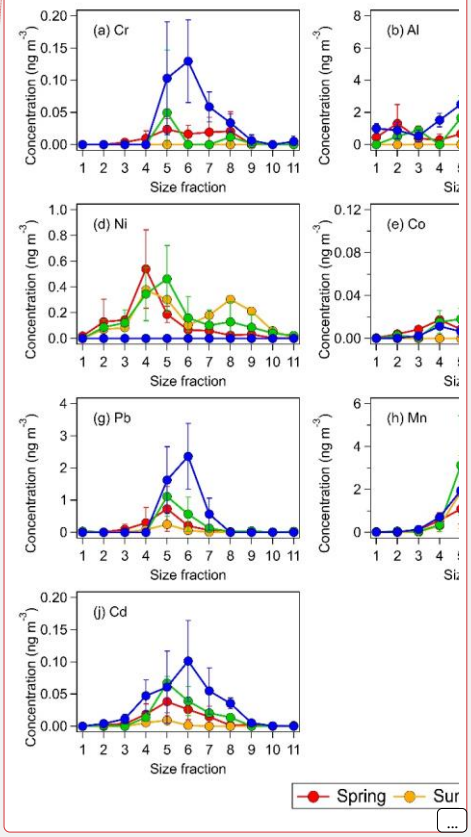

Deleted: with the followingdifferent nominal cut points

fraction 5), 1.0 µm (size fraction 6), 1.8 µm (size fraction 7), 3.2 µm (size fraction 8), 5.6 µm (size fraction 9), 10 µm (size fraction 10), and 18 µm (size fraction 11). The error bars represent one standard deviation of the seasonal average value.

Figure 2b shows the seasonal average mass concentrations of water-soluble metals in fine and coarse aerosols. Similar to the total metals, higher mass concentrations of water-soluble metals were usually measured during the winter and/or spring seasons. With the exception of Cu, the water-soluble metals usually had higher mass concentrations in fine aerosols than in coarse aerosols. The water-soluble metals generally had the same order of abundance as the total metals with some slight variations. The mass concentrations of water-soluble metals generally correlated with the mass concentrations of total metals (Table S2). This indicated that the water-soluble metals were largely derived from their total metals through atmospheric processing, and/or that water-soluble and water-insoluble metals have the same emission sources. For most of the metals, correlations between the mass concentrations of water-soluble and total metals were higher for fine aerosols than for coarse aerosols. This could be due to enhanced metal dissolution in fine aerosols via acid processing and/or the formation of stable metal-organic complexes, which are two atmospheric chemical processes that play key roles in influencing the solubilities of aerosol metals in many locations. This is because acidic inorganic species that promote acid processing and organic species that can serve as organic ligands are typically present in larger quantities in fine aerosols than in coarse aerosols. It is also possible that differences in metal mineralogy and atmospheric processing mechanisms in fine vs. coarse aerosols could have contributed to differences in the metal dissolution rates (Oakes et al., 2012; Longo et al., 2016; Ingall et al., 2018).

Figure 4 shows the study-averaged fractional solubilities for the ten metals in fine and coarse aerosols. The study-averaged metal fractional solubilities spanned a wide range for both fine (7.8 % to 71.2 %) and coarse (0.4 % to 47.9 %) aerosols. With the exception of Cu, the metals generally exhibited higher fractional solubilities in fine aerosols compared to coarse aerosols. The aerosol size-dependent metal fractional solubility could be explained by differences in the aerosol composition and metal mineralogy, which resulted in different metal dissolution rates and/or mechanisms for aerosols of different sizes. Our observations of mostly

Deleted: 8.8

Deleted: 70.3

Deleted: 1.4

Deleted: 54.3

Deleted: and Co

higher metal fractional solubilities in fine aerosols are consistent with previous studies conducted in Hong Kong and other locations worldwide (Baker et al., 2006; Jiang et al., 2014; Jiang et al., 2015; Fang et al., 2017; Gao et al., 2019; Baker et al., 2020; Gao et al., 2020b; Zhang et al., 2022). No season-dependent trend was observed for the metal fractional solubilities.

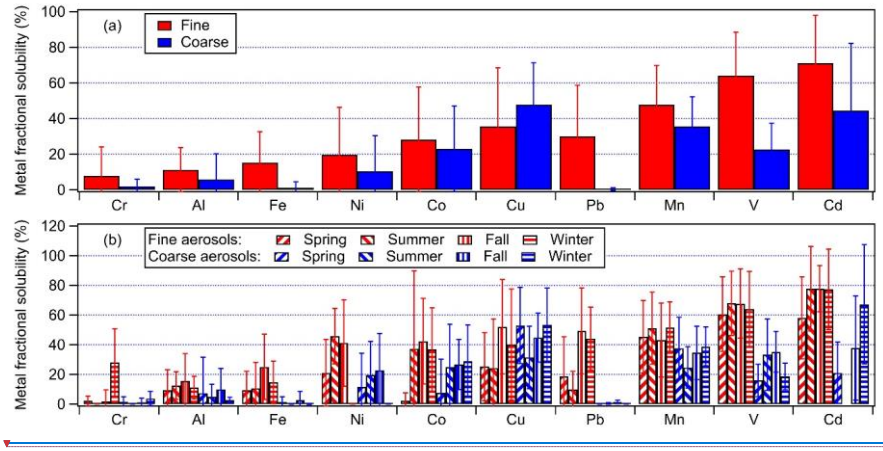

Figure 4: (a) Study-averaged fractional solubilities of metals in fine and coarse aerosols. (b) Seasonal average fractional solubilities of metals in fine and coarse aerosols. The error bars represent one standard deviation.

Some studies have reported that aerosol metal fractional solubilities will exhibit inverse relationships with the total metal concentrations as a result of atmospheric processing (Baker and Jickells, 2006; Sholkovitz et al., 2012; Mahowald et al., 2018; Shelley et al., 2018; Zhang et al., 2022). There was significant scatter in many of our datasets (Figure S6), which made it difficult to discern some of the relationships between the metal fractional solubilities and total metal concentrations. Inverse relationships between the fractional solubility and total metal concentration were noticeable for Cr, Al, Fe, Ni, Cu, Pb, and Mn. However, inverse relationships between the Co, V, and Cd fractional solubilities and their total metal concentrations were less noticeable due to their low concentrations and scatter in their datasets. A number of factors could have contributed to the scatter in the datasets. For instance, the scatter could be a result of the total and water-soluble metal concentrations being substantially

Deleted: in global scale

Deleted:

Deleted:

Deleted: S5

different in individual aerosol particles, which would not be captured by the bulk chemical analysis performed in this study (Oakes et al., 2012; Longo et al., 2016; Ingall et al., 2018). The metal dissolution rates in individual aerosol particles could also be significantly different due to differences in metal mineralogy, aerosol acidity levels, presence of organic ligands etc. in individual aerosol particles.

3.3. Factors that control the aerosol metal solubilities

Here, we identify the factors that control metal solubilities in fine aerosols since they are believed to exert higher toxicity than coarse aerosols due to their small sizes. Our analyses focus on aerosol metal dissolution via metal-organic complexation reactions and acid processing, which are two atmospheric chemical processes believed to drive aerosol metal dissolution in most environments. Laboratory studies have shown that the presence of organic ligands enhances Fe dissolution in aerosols (Paris et al., 2011; Chen and Grassian, 2013; Paris and Desboeufs, 2013; Wang et al., 2017). Water-soluble dicarboxylic acids, especially oxalate, form stable complexes with Fe ions, which will lower the energy barrier for Fe dissolution. While evidence of organic ligand-promoted metal dissolution in ambient aerosols has been less conclusive, recent field studies compared the oxalate and water-soluble Fe concentrations to show that the presence of organic ligands could contribute to aerosol Fe solubility. For instance, strong positive correlations between oxalate and water-soluble Fe mass concentrations were observed for $PM_{2.5}$ collected at six urban and rural sites in Canada (Tao and Murphy, 2019). The Fe fractional solubility was also observed to be positively correlated with the molar ratio of oxalate and Fe for $PM_{2.5}$ collected at a suburban site in Qingdao, China (Zhang et al., 2022).

To investigate whether organic ligands influenced aerosol metal solubilities in this study, we attempted to measure oxalate in the size-fractionated aerosol samples using IC. However, we could not detect oxalate, which indicated that the concentrations of oxalate (if present) were below the detection limits of our IC instrument. It should be noted that although a recent study reported the copresence of Fe and oxalate in individual aerosol particles at a suburban site in Hong Kong using single particle mass spectrometry (Zhou et al., 2020), organic ligand-promoted metal dissolution is a slow process, and it plays a minor role in metal dissolution

Deleted: Even though oxalate was not detected in our size-fractionated aerosol samples, the possibility that organic ligand-promoted dissolution contributed partly to the aerosol metal solubilities cannot be discounted completely. Oxalate concentrations of up to about 0.5 μg m^{-3} have previously been reported in $PM_{2.5}$ in Hong Kong. In addition,

Deleted: . However

Deleted: O

499 under low pH conditions (Zhu et al., 1993). The fine aerosols collected in this study were
500 mostly acidic, with about 60 % of the calculated pH values being less than 3. This suggested
501 that organic ligand-promoted dissolution may have played a minor role in enhancing aerosol
502 metal solubilities in this study due to the acidic nature of the aerosols.

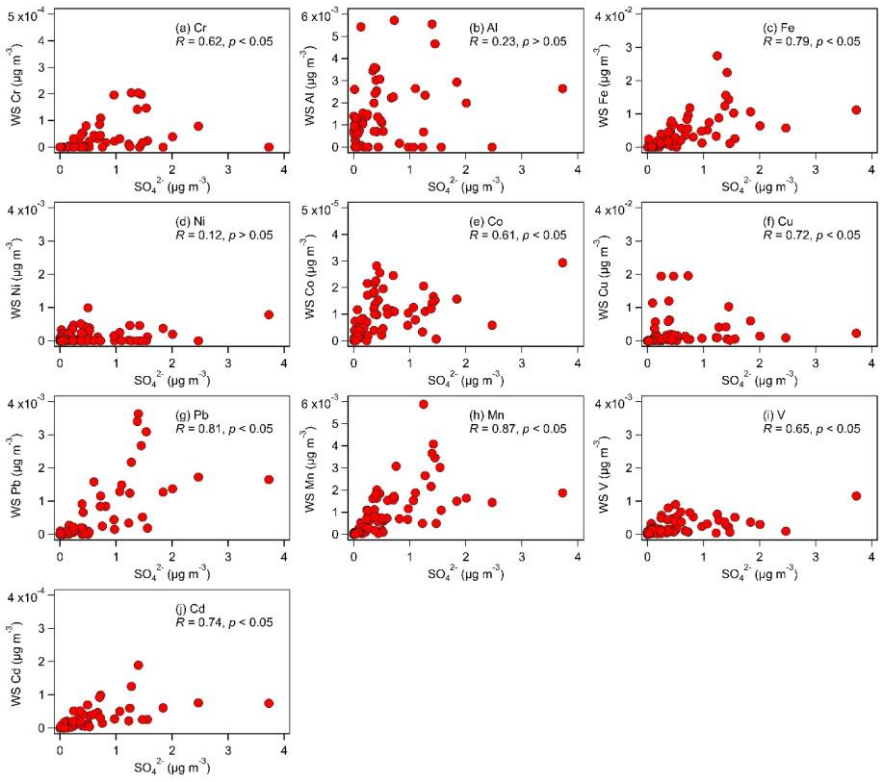

503

504 **Figure 5:** Relationships between the mass concentrations of water-soluble (WS) metals and
505 sulfate in fine aerosols. Only data with non-zero total metal concentrations were used in the
506 figures. Also shown are the spearman correlation coefficients for each relationship.

507 The acidic nature of the aerosols raises the possibility that acid processing played a
508 major role in enhancing aerosol metal solubilities. A previous study that utilized nanoscale
509 single-particle mass spectrometric and imaging techniques to analyze the mixing states of Fe-
510 containing aerosols collected over the East China Sea provided insights into the mechanism of

Fe dissolution by acidic species that condensed onto atmospheric aerosols (Li et al., 2017). The authors reported that Fe oxide-rich aerosols emitted from steel plants and coal combustion were coated with thick layers of acidic sulfate after 1 to 2 days of atmospheric aging. These sulfate coatings originated from the condensation of sulfuric acid, which were formed from reactions of anthropogenic SO_2. While the fresh aerosols were composed primarily of insoluble Fe oxide, the aged aerosols contained soluble Fe sulfate that were internally mixed in the sulfate coatings. Although the mechanism proposed by Li et al. (2017) focused on explaining how sulfate-driven acid processing leads to the dissolution of the water-insoluble forms Fe, this mechanism likely applies to the other aerosol metals as well. During acid processing, acidic species have to overcome the buffering capacity of the aqueous aerosol particle to raise the aerosol acidity level to the point where the dissolution of metal species is thermodynamically favored. Sulfate was the most abundant aqueous-phase acidic species in our size-fractionated aerosol samples. The concentrations of nitrate (another aqueous-phase acidic species) were very low (about 18 times lower than sulfate, on average), while aqueous-phase organic acids were not detected. Hence, we first analyzed the relationships between the concentrations of water-soluble metals and sulfate. Figure 5 shows that despite the scatter in the datasets, the concentrations of water-soluble metals were positively correlated with the concentration of sulfate, though the correlations between the concentrations of sulfate and water-soluble Al and Ni were not statistically significant. These positive correlations could be due, in part, to the water-soluble metals and sulfate precursor (i.e., SO_2) being emitted from the same sources. However, the masses of primary water-soluble aerosol metals are not known. The positive correlations could also be due to the role that sulfate plays in aerosol metal dissolution during acid processing.

Deleted: Since sulfate is the main aqueous-phase acidic species in fine aerosols in Hong Kong

To investigate the roles that sulfate and nitrate played in controlling aerosol metal solubilities, we analyzed the relationships between the metal fractional solubilities and sulfate and nitrate concentrations. In general, the correlations between the metal fractional solubilities and sulfate concentration (Table 1) were substantially higher than the correlations between the metal fractional solubilities and nitrate concentration (Table S3). This implied that sulfate likely plays a more important role than nitrate in controlling aerosol metal solubilities, which is not surprising given the low concentrations of nitrate detected (about 18 times lower than sulfate,

on average). Analyses of the correlations between the metal fractional solubilities and sulfate concentration (Table 1 and Figure 6) indicated that the Cr, Fe, Co, Cu, Pb, and Mn fractional solubilities were positively correlated with the sulfate concentration, and these correlations were statistically significant. This implied that sulfate played a key role in the formation of water-soluble Cr, Fe, Co, Cu, Pb, and Mn, likely though sulfate-driven acid dissolution of their water-insoluble forms. Conversely, the positive correlations between the sulfate concentration and the Al, Ni, V, and Cd fractional solubilities were weak and not statistically significant. Interestingly, the V and Cd fractional solubilities showed weak correlations with the sulfate concentration ($R = 0.14$ and $R = 0.04$, respectively), whereas their water-soluble concentrations showed strong correlations with the sulfate concentration ($R = 0.65$ and $R = 0.74$, respectively). It is possible that the strong correlations of sulfate concentration with water-soluble V and Cd concentrations but not with V and Cd fractional solubilities were due to a large fraction of water-soluble V and Cd having the same sources as sulfate and its precursor (i.e., SO_2). For instance, Celo et al. (2015) reported that substantial concentrations of water-soluble aerosol metals (including V), sulfate, and SO_2 are present in exhaust emissions from the main engines of commercial marine vessels.

Deleted: emission

Deleted: the

Table 1: Spearman rank correlations between the metal fractional solubilities and W_i and H^+_{air} in fine aerosols[a]

Metal	Sulfate	W_i	H^+_{air}	pH
Cr	**0.62**	**0.42**	**0.48**	-0.16
Al	0.14	0.08	0.14	-0.06
Fe	**0.53**	**0.31**	**0.50**	**-0.33**
Ni	0.03	0.01	0.18	**-0.26**
Co	**0.41**	**0.41**	**0.23**	-0.05
Cu	**0.74**	**0.72**	**0.24**	-0.07
Pb	**0.53**	**0.41**	**0.34**	-0.13
Mn	**0.49**	**0.43**	**0.23**	-0.01
V	0.14	0.01	0.21	-0.20
Cd	0.04	0.10	0.13	0.22

[a] Bold: statistically significant ($p < 0.05$)

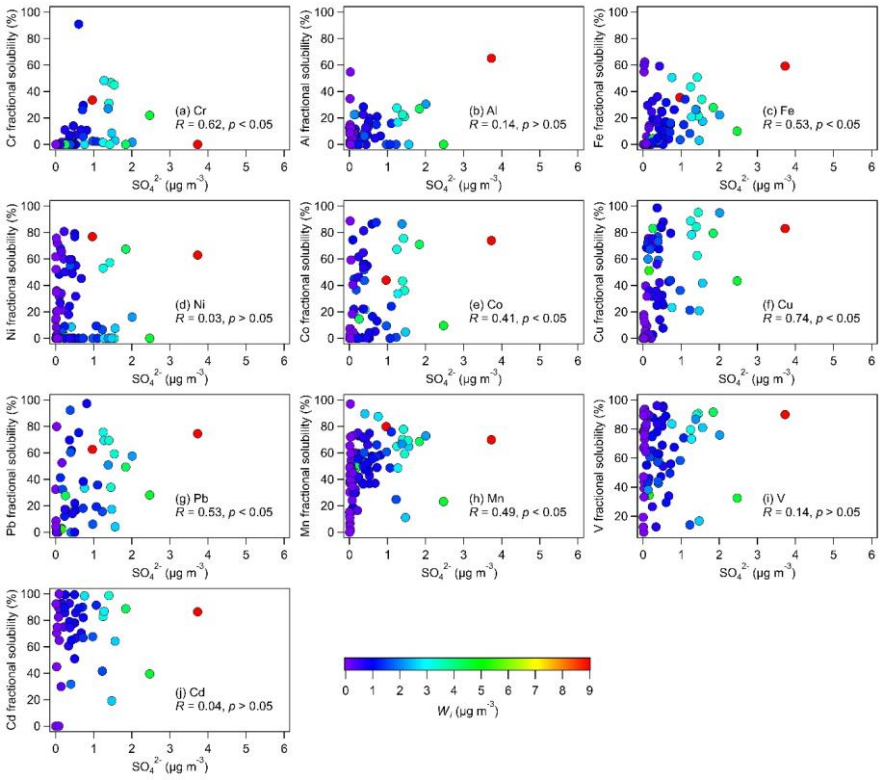

Figure 6: Relationships between the metal fractional solubilities and sulfate mass concentration in fine aerosols. Only data with non-zero total metal concentrations were used in the figures. Also shown are the spearman correlation coefficients for each relationship. The symbols are colored by the corresponding W_i concentrations calculated by ISORROPIA-II. The W_i concentrations increased with sulfate concentrations.

High levels of aerosol acidity and liquid water are generally needed for the acid dissolution of metals in an aqueous aerosol particle. In addition to being the main contributor to aerosol acidity levels (i.e., H^+_{air}), sulfate is a highly hygroscopic species that will influence the overall aerosol water uptake behavior, which will drive W_i. Sulfate was the main driver of W_i in fine aerosols in our study since the mass concentrations of nitrate (another highly hygroscopic species) were very low (about 18 times lower than sulfate, on average). Both W_i and H^+_{air} were controlled primarily by sulfate (sulfate and W_i R = 0.90, p < 0.05; sulfate and

H^+_{air} R = 0.63, p < 0.05). Thus, we analyzed the relationships between the aerosol metal fractional solubilities and W_i and H^+_{air} (Figures S7 and S8). Table 1 shows that correlations between the Al, Ni, V, and Cd fractional solubilities and W_i and H^+_{air} were weak. Together, the weak correlations between the fractional solubilities of Al, Ni, V, and Cd and sulfate, W_i, and H^+_{air} implied that acid processing may have played a minor role in enhancing the solubilities of these four metals. Other atmospheric processes beyond acid processing (e.g., cloud processing, photoreduction) could have played more important roles in enhancing the solubilities of these four metals (Zhu et al., 1993; Spokes et al., 1994; Kuma et al., 1995). It is possible that these four metals had slow acid dissolution rates as a result of their mineralogy and oxidation states. The impacts of mineralogy and oxidation states on the susceptibilities of water-insoluble Al, Ni, V, and Cd to acid dissolution are currently not known. However, previous studies showed that different aerosol Fe mineralogy and oxidation states have different susceptibilities to acid dissolution that will occur at different timescales (Ingall et al., 2018). Hence, analogous to Fe, it is possible that the mineralogy and oxidation states of Al, Ni, V, and Cd in the collected aerosols may have resulted in these four metals being less susceptible to acid processing, which in turn caused them to undergo slow sulfate-driven acid dissolution from water-insoluble forms to water-soluble forms.

Table 1 shows that the Cr, Fe, Co, Cu, Pb, and Mn fractional solubilities were positively correlated with W_i and H^+_{air}, and these correlations were statistically significant. Together, the statistically significant positive correlations between the fractional solubilities of Cr, Fe, Co, Cu, Pb, and Mn and sulfate, W_i, and H^+_{air} indicated that acid processing likely played an important role in enhancing the solubilities of these six metals. The fractional solubilities of Co, Cu, Pb, and Mn were more strongly correlated with the W_i concentration than with the H^+_{air} concentration. This suggested that W_i had a stronger influence on the acid dissolution of Co, Cu, Pb, and Mn. The strong influence that W_i has on the metal fractional solubility could be explained by the role of aerosol water as a reaction medium for the acid dissolution of metals in an aqueous aerosol particle. Wong et al. (2020) previously showed that at a relatively constant aerosol pH, a decrease in W_i will lead to a decrease in the reaction medium volume, which in turn will lead to decreases in the overall formation rates of water-soluble metals.

Deleted: 6

Deleted: S7

Deleted: strong

Deleted: a major

609 Conversely, the fractional solubilities of Cr and Fe were more strongly correlated with the H^+_{air}
610 concentration than with the W_i concentration. This suggested that the aerosol acidity levels had
611 a stronger influence on the acid dissolution of Cr and Fe. Despite the statistically significant
612 positive correlations between the fractional solubilities of Cr, Fe, Co, Cu, Pb, and Mn and
613 sulfate, W_i, and H^+_{air} (Table 1), there was significant scatter in the datasets (Figures 6, S7, and
614 S8). This scatter could be a result of the sulfate, W_i, H^+_{air}, total and water-soluble metal
615 concentrations being substantially different in individual aerosol particles, which would not be
616 captured by the bulk chemical analysis and thermodynamic modeling performed in this study.
617 The metal dissolution rates in individual aerosol particles could also be significantly different
618 due to differences in metal mineralogy, aerosol acidity levels, etc. in individual aerosol particles.
619 In addition, a recent study by Yang et al. (2021) reported that the filterable metal fractions in
620 the water extracts may contain some metals in water-insoluble forms with small diameters that
621 allowed them to pass through the pores of syringe filters. This would result in over-estimated
622 metal fractional solubilities, which could explain why some of the data points in Figure 6
623 showed high metal fractional solubilities at low sulfate concentrations.

624 Interestingly, variability in the aerosol pH did not appear to be a key driver of the
625 variability in the solubilities of Cr, Fe, Co, Cu, Pb, and Mn. It was difficult to discern aerosol
626 pH-dependent fractional solubility trends for these six metals, and their fractional solubilities
627 were not highly correlated with aerosol pH (Table 1 and Figure S9). This could be attributed
628 partly to the scatter in the datasets caused by differences in the metal solubilities and pH in
629 individual aerosol particles that would not be captured by the bulk chemical analysis and
630 thermodynamic modeling performed in this study. The absence of obvious aerosol pH-
631 dependent fractional solubility trends could also be due to the insensitivity of aerosol pH to the
632 variability of sulfate ($R = -0.22$, $p < 0.05$). Based on Equation (1), the aerosol pH could be
633 viewed simply as the ratio of H^+_{air} and W_i. Both W_i and H^+_{air} were highly variable in this study,
634 and both were controlled primarily by sulfate. As a result, the ratio of H^+_{air} and W_i, or the
635 aerosol pH, would be fairly insensitive to sulfate even though it was driven primarily by sulfate.
636 Previous studies have similarly reported weak or the absence of aerosol pH-dependent metal
637 fractional solubility trends despite evidence of aerosol metal dissolution being enhanced by

Deleted: S8

acid processing (Shi et al., 2020; Wong et al., 2020).

4. Conclusions

In this study, we investigated the abundance and fractional solubilities of ten metals (Fe, Cu, Al, V, Cr, Mn, Co, Ni, Cd, and Pb) in size-fractionated aerosols collected at an urban site in Hong Kong. Weekly aerosol samples were collected for a month during different seasons from March 2021 to January 2022. The main objective of this study was to identify the key factors that controlled metal solubilities in fine aerosols, with a focus on aerosol metal dissolution via the acid processing and metal-organic complexation mechanisms. Hence, other aerosol chemical species were measured in addition to the total and water-soluble metals.

Higher mass concentrations of total metals were usually measured during the winter and/or spring seasons. This was likely due to the long-range transport of polluted air masses by northly prevailing winds from emission sources located in continental areas north of Hong Kong. The total metals could be arranged in the following order based on their abundances: Fe > Al > Cu > Co > Mn > Pb > Cr > Ni > V > Cd. This order of abundance was the same for both fine and coarse aerosols. The major sources of the total metals were sea salt, dust, ship emissions, and industrial activities. Higher mass concentrations of water-soluble metals were also usually measured during the winter and/or spring seasons. With the exception of Cu, the water-soluble metals had higher mass concentrations in fine aerosols than in coarse aerosols. The mass concentrations of water-soluble metals generally correlated with the mass concentrations of total metals, which implied that the water-soluble metals were largely derived from their total metals through atmospheric processing and/or that water-soluble and water-insoluble metals have the same emission sources. The study-averaged metal fractional solubilities spanned a wide range for both fine (7.8 % to 71.2 %) and coarse (0.4 % to 47.9 %) aerosols. With the exception of Cu and Co, the metals exhibited higher fractional solubilities in fine aerosols compared to coarse aerosols. The aerosol size-dependent metal fractional solubility could potentially be attributed to differences in the composition and metal mineralogy which resulted in different metal dissolution rates and/or mechanisms for aerosols of different sizes.

Deleted: Fe > Al > Cu > Mn > Pb > Ni > Cr > V > Co > Cd

Deleted: 8.8 % to 70.3 %

Deleted: 1.4 % to 54.3 %

The fine aerosols collected in this study were mostly acidic, with about 60 % of the calculated pH values below 3. The acidic nature of the fine aerosols combined with oxalate (which forms metal-organic complexes easily) not being detected in our aerosol samples suggested that organic ligand-promoted dissolution likely played a minor role in enhancing aerosol metal solubilities. This is because organic ligand-promoted metal dissolution is a slow process, and it plays a minor role in metal dissolution under low pH conditions. Our analyses showed that sulfate, which is the dominant fine aerosol acidic species, exhibited statistically significant positive correlations with both the water-soluble concentrations of Cr, Fe, Co, Cu, Pb, and Mn and their fractional solubilities. In addition, sulfate controlled W_i and H^+_{air}, both of which are needed for acid dissolution of metals in an aqueous aerosol particle. The water-soluble concentrations of Cr, Fe, Co, Cu, Pb, and Mn and their fractional solubilities exhibited statistically significant positive correlations with both W_i and H^+_{air}. Together, the statistically significant positive correlations between the fractional solubilities of Cr, Fe, Co, Cu, Pb, and Mn and sulfate, W_i, and H^+_{air} indicated that acid processing likely played an important role in enhancing the solubilities of these six metals. The fractional solubilities of Co, Cu, Pb, and Mn were more strongly correlated with the W_i concentration than with the H^+_{air} concentration, which implied that W_i had a stronger influence on the acid dissolution of these four metals. The fractional solubilities of Cr and Fe were more strongly correlated with the H^+_{air} concentration than with the W_i concentration, which implied that the aerosol acidity levels had a stronger influence on the acid dissolution of these two metals. Conversely, our analyses suggested that acid processing played a minor role in enhancing the solubilities of Al, Ni, V, and Cd. It is possible that the mineralogy and oxidation states of these four metals made them less susceptible to acid processing.

Deleted: strong

Deleted: major

In conclusion, this study highlights the key role that sulfate plays in controlling the solubilities of a host of metals in fine aerosols (in this case, Cr, Fe, Co, Cu, Pb, and Mn). This is mostly due to sulfate's ability to both strongly acidify the aerosol particle and provide the liquid reaction medium needed for the acid dissolution of metals. Although this study was performed at an urban site in Hong Kong, we expect our findings to broadly apply to other urban areas in Hong Kong and South China, where sulfate is the dominant acidic and

hygroscopic component in fine aerosols. Results from this study can also provide insights into how the solubilities of different aerosol metals will change with the decrease in sulfate as Hong Kong and other cities in South China transition away from coal combustion as their main energy source to improve local and regional air quality and combat climate change.

Data availability: The data used in this publication is available to the community and can be accessed at: https://doi.org/10.5281/zenodo.7013770 (Yang et al., 2022).

Author contributions: J.Y. and T.N. designed the study. J.Y. collected the field samples. J.Y., L.M., and W.C.A. performed chemical analysis of the field samples. J.Y., X.H., Y.M., and T.N. analyzed the data. J.Y. and T.N. prepared the manuscript with contributions from all co-authors.

Competing interests: One of the authors is a member of the editorial board of *Atmospheric Chemistry and Physics*. The peer-review process was guided by an independent editor, and the authors also have no other competing interests to declare.

Acknowledgements: This work was supported by the Research Grants Council of Hong Kong (project number 21304919).

References

Adachi, K. and Tainosho, Y.: Characterization of heavy metal particles embedded in tire dust, Environment International, 30, 1009-1017, https://doi.org/10.1016/j.envint.2004.04.004, 2004.

Al-Abadleh, H. A.: Review of the bulk and surface chemistry of iron in atmospherically relevant systems containing humic-like substances, Rsc Advances, 5, 45785-45811, https://doi.org/10.1039/c5ra03132j, 2015.

Al-Abadleh, H. A.: Aging of atmospheric aerosols and the role of iron in catalyzing brown carbon formation, Environmental Science: Atmospheres, 1, 297-345, 10.1039/D1EA00038A, 2021.

Baker, A. R. and Jickells, T. D.: Mineral particle size as a control on aerosol iron solubility, Geophysical Research Letters, 33, https://doi.org/10.1029/2006GL026557, 2006.

Baker, A. R., Li, M., and Chance, R.: Trace Metal Fractional Solubility in Size-Segregated Aerosols From the Tropical Eastern Atlantic Ocean, Global Biogeochemical Cycles, 34, e2019GB006510, https://doi.org/10.1029/2019GB006510, 2020.

Baker, A. R., Jickells, T. D., Witt, M., and Linge, K. L.: Trends in the solubility of iron,

aluminium, manganese and phosphorus in aerosol collected over the Atlantic Ocean, Marine Chemistry, 98, 43-58, https://doi.org/10.1016/j.marchem.2005.06.004, 2006.

Bates, J. T., Fang, T., Verma, V., Zeng, L. H., Weber, R. J., Tolbert, P. E., Abrams, J. Y., Sarnat, S. E., Klein, M., Mulholland, J. A., and Russell, A. G.: Review of Acellular Assays of Ambient Particulate Matter Oxidative Potential: Methods and Relationships with Composition, Sources, and Health Effects, Environmental Science & Technology, 53, 4003-4019, https://doi.org/10.1021/acs.est.8b03430, 2019.

Birmili, W., Allen, A. G., Bary, F., and Harrison, R. M.: Trace Metal Concentrations and Water Solubility in Size-Fractionated Atmospheric Particles and Influence of Road Traffic, Environmental Science & Technology, 40, 1144-1153, https://doi.org/10.1021/es0486925, 2006.

Boyd, P. W., Jickells, T., Law, C. S., Blain, S., Boyle, E. A., Buesseler, K. O., Coale, K. H., Cullen, J. J., de Baar, H. J. W., Follows, M., Harvey, M., Lancelot, C., Levasseur, M., Owens, N. P. J., Pollard, R., Rivkin, R. B., Sarmiento, J., Schoemann, V., Smetacek, V., Takeda, S., Tsuda, A., Turner, S., and Watson, A. J.: Mesoscale iron enrichment experiments 1993-2005: Synthesis and future directions, Science, 315, 612-617, https://doi.org/10.1126/science.1131669, 2007.

Bresgen, N. and Eckl, P. M.: Oxidative stress and the homeodynamics of iron metabolism, Biomolecules, 5, 808-847, https://doi.org/10.3390/biom5020808, 2015.

Brook, R. D., Rajagopalan, S., Pope, C. A., Brook, J. R., Bhatnagar, A., Diez-Roux, A. V., Holguin, F., Hong, Y. L., Luepker, R. V., Mittleman, M. A., Peters, A., Siscovick, D., Smith, S. C., Whitsel, L., Kaufman, J. D., Amer Heart Assoc Council, E., Council Kidney Cardiovasc, D., and Council Nutr Phys Activity, M.: Particulate Matter Air Pollution and Cardiovascular Disease An Update to the Scientific Statement From the American Heart Association, Circulation, 121, 2331-2378, https://doi.org/10.1161/CIR.0b013e3181dbece1, 2010.

Celo, V., Dabek-Zlotorzynska, E., and McCurdy, M.: Chemical Characterization of Exhaust Emissions from Selected Canadian Marine Vessels: The Case of Trace Metals and Lanthanoids, Environmental Science & Technology, 49, 5220-5226, https://doi.org/10.1021/acs.est.5b00127, 2015.

Chen, H. H. and Grassian, V. H.: Iron Dissolution of Dust Source Materials during Simulated Acidic Processing: The Effect of Sulfuric, Acetic, and Oxalic Acids, Environmental Science & Technology, 47, 10312-10321, https://doi.org/10.1021/es401285s, 2013.

Cheng, Y., Lee, S. C., Cao, J., Ho, K. F., Chow, J., Watson, J., and Ao, C.: Elemental composition of airborne aerosols at a traffic site and a suburban site in Hong Kong, International Journal of Environment and Pollution, 36, 166-179, 2009.

Chow, W. S., Huang, X. H. H., Leung, K. F., Huang, L., Wu, X., and Yu, J. Z.: Molecular and elemental marker-based source apportionment of fine particulate matter at six sites in Hong

Kong, China, Science of The Total Environment, 813, 152652, https://doi.org/10.1016/j.scitotenv.2021.152652, 2022.

Chu, B., Hao, J., Li, J., Takekawa, H., Wang, K., and Jiang, J.: Effects of two transition metal sulfate salts on secondary organic aerosol formation in toluene/NOxphotooxidation, Frontiers of Environmental Science & Engineering, 7, 1-9, https://doi.org/10.1007/s11783-012-0476-x, 2013.

Chu, B., Liggio, J., Liu, Y., He, H., Takekawa, H., Li, S.-M., and Hao, J.: Influence of metal-mediated aerosol-phase oxidation on secondary organic aerosol formation from the ozonolysis and OH-oxidation of α-pinene, Scientific Reports, 7, 40311, https://doi.org/10.1038/srep40311, 2017.

Cohen, A. J., Brauer, M., Burnett, R., Anderson, H. R., Frostad, J., Estep, K., Balakrishnan, K., Brunekreef, B., Dandona, L., Dandona, R., Feigin, V., Freedman, G., Hubbell, B., Jobling, A., Kan, H., Knibbs, L., Liu, Y., Martin, R., Morawska, L., Pope, C. A., Shin, H., Straif, K., Shaddick, G., Thomas, M., van Dingenen, R., van Donkelaar, A., Vos, T., Murray, C. J. L., and Forouzanfar, M. H.: Estimates and 25-year trends of the global burden of disease attributable to ambient air pollution: an analysis of data from the Global Burden of Diseases Study 2015, Lancet, 389, 1907-1918, https://doi.org/10.1016/s0140-6736(17)30505-6, 2017.

Costa, D. L. and Dreher, K. L.: Bioavailable transition metals in particulate matter mediate cardiopulmonary injury in healthy and compromised animal models, Environmental Health Perspectives, 105, 1053-1060, https://doi.org/10.2307/3433509, 1997a.

Costa, D. L. and Dreher, K. L.: Bioavailable transition metals in particulate matter mediate cardiopulmonary injury in healthy and compromised animal models, Environmental Health Perspectives, 105, 1053-1060, https://doi.org/10.1289/ehp.97105s51053, 1997b.

de Baar, H. J. W., Boyd, P. W., Coale, K. H., Landry, M. R., Tsuda, A., Assmy, P., Bakker, D. C. E., Bozec, Y., Barber, R. T., Brzezinski, M. A., Buesseler, K. O., Boye, M., Croot, P. L., Gervais, F., Gorbunov, M. Y., Harrison, P. J., Hiscock, W. T., Laan, P., Lancelot, C., Law, C. S., Levasseur, M., Marchetti, A., Millero, F. J., Nishioka, J., Nojiri, Y., van Oijen, T., Riebesell, U., Rijkenberg, M. J. A., Saito, H., Takeda, S., Timmermans, K. R., Veldhuis, M. J. W., Waite, A. M., and Wong, C. S.: Synthesis of iron fertilization experiments: From the iron age in the age of enlightenment, Journal of Geophysical Research-Oceans, 110, https://doi.org/10.1029/2004jc002601, 2005.

Deguillaume, L., Leriche, M., Desboeufs, K., Mailhot, G., George, C., and Chaumerliac, N.: Transition Metals in Atmospheric Liquid Phases: Sources, Reactivity, and Sensitive Parameters, Chemical Reviews, 105, 3388-3431, https://doi.org/10.1021/cr040649c, 2005.

Fang, T., Guo, H., Verma, V., Peltier, R. E., and Weber, R. J.: PM2.5 water-soluble elements in the southeastern United States: automated analytical method development, spatiotemporal distributions, source apportionment, and implications for heath studies, Atmos. Chem. Phys., 15, 11667-11682, https://doi.org/10.5194/acp-15-11667-2015, 2015.

Fang, T., Guo, H., Zeng, L., Verma, V., Nenes, A., and Weber, R. J.: Highly Acidic Ambient Particles, Soluble Metals, and Oxidative Potential: A Link between Sulfate and Aerosol Toxicity, Environmental Science & Technology, 51, 2611-2620, https://doi.org/10.1021/acs.est.6b06151, 2017.

Fountoukis, C. and Nenes, A.: ISORROPIA II: a computationally efficient thermodynamic equilibrium model for K+–Ca2+–Mg2+–NH4+–Na+–SO42−–NO3−–Cl−–H2O aerosols, Atmos. Chem. Phys., 7, 4639-4659, https://doi.org/10.5194/acp-7-4639-2007, 2007.

Fountoukis, C., Nenes, A., Sullivan, A., Weber, R., Van Reken, T., Fischer, M., Matias, E., Moya, M., Farmer, D., and Cohen, R. C.: Thermodynamic characterization of Mexico City aerosol during MILAGRO 2006, Atmospheric Chemistry and Physics, 9, 2141-2156, https://doi.org/10.5194/acp-9-2141-2009, 2009.

Frampton, M. W., Ghio, A. J., Samet, J. M., Carson, J. L., Carter, J. D., and Devlin, R. B.: Effects of aqueous extracts of PM10 filters from the Utah Valley on human airway epithelial cells, American Journal of Physiology-Lung Cellular and Molecular Physiology, 277, L960-L967, https://doi.org/10.1152/ajplung.1999.277.5.L960, 1999.

Gao, D., Mulholland, J. A., Russell, A. G., and Weber, R. J.: Characterization of water-insoluble oxidative potential of PM2.5 using the dithiothreitol assay, Atmospheric Environment, 224, https://doi.org/10.1016/j.atmosenv.2020.117327, 2020a.

Gao, Y., Yu, S., Sherrell, R. M., Fan, S., Bu, K., and Anderson, J. R.: Particle-Size Distributions and Solubility of Aerosol Iron Over the Antarctic Peninsula During Austral Summer, Journal of Geophysical Research: Atmospheres, 125, e2019JD032082, https://doi.org/10.1029/2019JD032082, 2020b.

Gao, Y., Marsay, C. M., Yu, S., Fan, S., Mukherjee, P., Buck, C. S., and Landing, W. M.: Particle-Size Variability of Aerosol Iron and Impact on Iron Solubility and Dry Deposition Fluxes to the Arctic Ocean, Scientific Reports, 9, 16653, https://doi.org/10.1038/s41598-019-52468-z, 2019.

Garg, B. D., Cadle, S. H., Mulawa, P. A., Groblicki, P. J., Laroo, C., and Parr, G. A.: Brake Wear Particulate Matter Emissions, Environmental Science & Technology, 34, 4463-4469, https://doi.org/10.1021/es001108h, 2000.

Garrett, R. G.: Natural Sources of Metals to the Environment, Human and Ecological Risk Assessment: An International Journal, 6, 945-963, https://doi.org/10.1080/10807030091124383, 2000.

Giorio, C., D'Aronco, S., Di Marco, V., Badocco, D., Battaglia, F., Soldà, L., Pastore, P., and Tapparo, A.: Emerging investigator series: aqueous-phase processing of atmospheric aerosol influences dissolution kinetics of metal ions in an urban background site in the Po Valley, Environmental Science: Processes & Impacts, 24, 884-897, http://dx.doi.org/10.1039/D2EM00023G, 2022.

He, X., Liu, P., Zhao, W., Xu, H., Zhang, R., and Shen, Z.: Size distribution of water-soluble metals in atmospheric particles in Xi'an, China: Seasonal variations, bioavailability, and health risk assessment, Atmospheric Pollution Research, 12, 101090, https://doi.org/10.1016/j.apr.2021.101090, 2021.

Heal, M. R., Elton, R. A., Hibbs, L. R., Agius, R. M., and Beverland, I. J.: A time-series study of the health effects of water-soluble and total-extractable metal content of airborne particulate matter, Occupational and Environmental Medicine, 66, 636-638, https://doi.org/10.1136/oem.2008.045310, 2009.

Hopke, P. K., Lamb, R. E., and Natusch, D. F. S.: Multielemental characterization of urban roadway dust, Environmental Science & Technology, 14, 164-172, https://doi.org/10.1021/es60162a006, 1980.

Ingall, E. D., Feng, Y., Longo, A. F., Lai, B., Shelley, R. U., Landing, W. M., Morton, P. L., Nenes, A., Mihalopoulos, N., Violaki, K., Gao, Y., Sahai, S., and Castorina, E.: Enhanced Iron Solubility at Low pH in Global Aerosols, Atmosphere, 9, 201, 2018.

Jiang, S. Y., Kaul, D. S., Yang, F., Sun, L., and Ning, Z.: Source apportionment and water solubility of metals in size segregated particles in urban environments, Science of The Total Environment, 533, 347-355, https://doi.org/10.1016/j.scitotenv.2015.06.146, 2015.

Jiang, S. Y. N., Yang, F., Chan, K. L., and Ning, Z.: Water solubility of metals in coarse PM and PM2.5 in typical urban environment in Hong Kong, Atmospheric Pollution Research, 5, 236-244, https://doi.org/10.5094/APR.2014.029, 2014.

Jordi, A., Basterretxea, G., Tovar-Sanchez, A., Alastuey, A., and Querol, X.: Copper aerosols inhibit phytoplankton growth in the Mediterranean Sea, Proceedings of the National Academy of Sciences of the United States of America, 109, 21246-21249, https://doi.org/10.1073/pnas.1207567110, 2012.

Kuma, K., Nakabayashi, S., and Matsunaga, K.: Photoreduction of Fe(III) by hydroxycarboxylic acids in seawater, Water Research, 29, 1559-1569, https://doi.org/10.1016/0043-1354(94)00289-J, 1995.

Lakey, P. S. J., Berkemeier, T., Tong, H. J., Arangio, A. M., Lucas, K., Poschl, U., and Shiraiwa, M.: Chemical exposure-response relationship between air pollutants and reactive oxygen species in the human respiratory tract, Scientific Reports, 6, https://doi.org/10.1038/srep32916, 2016.

Lee, C. S. L., Li, X.-D., Zhang, G., Li, J., Ding, A.-J., and Wang, T.: Heavy metals and Pb isotopic composition of aerosols in urban and suburban areas of Hong Kong and Guangzhou, South China—Evidence of the long-range transport of air contaminants, Atmospheric Environment, 41, 432-447, https://doi.org/10.1016/j.atmosenv.2006.07.035, 2007.

Li, W., Wang, T., Zhou, S., Lee, S., Huang, Y., Gao, Y., and Wang, W.: Microscopic Observation

878 of Metal-Containing Particles from Chinese Continental Outflow Observed from a Non-
879 Industrial Site, Environmental Science & Technology, 47, 9124-9131,
880 https://doi.org/10.1021/es400109q, 2013.

881 Li, W., Xu, L., Liu, X., Zhang, J., Lin, Y., Yao, X., Gao, H., Zhang, D., Chen, J., Wang, W.,
882 Harrison, R. M., Zhang, X., Shao, L., Fu, P., Nenes, A., and Shi, Z.: Air pollution–aerosol
883 interactions produce more bioavailable iron for ocean ecosystems, Science Advances, 3,
884 e1601749, https://doi.org/10.1126/sciadv.1601749, 2017.

885 Lippmann, M.: Toxicological and epidemiological studies of cardiovascular effects of ambient
886 air fine particulate matter (PM2.5) and its chemical components: Coherence and public health
887 implications, Critical Reviews in Toxicology, 44, 299-347,
888 https://doi.org/10.3109/10408444.2013.861796, 2014.

889 Longo, A. F., Feng, Y., Lai, B., Landing, W. M., Shelley, R. U., Nenes, A., Mihalopoulos, N.,
890 Violaki, K., and Ingall, E. D.: Influence of Atmospheric Processes on the Solubility and
891 Composition of Iron in Saharan Dust, Environmental Science & Technology, 50, 6912-6920,
892 https://doi.org/10.1021/acs.est.6b02605, 2016.

893 Lough, G. C., Schauer, J. J., Park, J.-S., Shafer, M. M., DeMinter, J. T., and Weinstein, J. P.:
894 Emissions of Metals Associated with Motor Vehicle Roadways, Environmental Science &
895 Technology, 39, 826-836, https://doi.org/10.1021/es048715f, 2005.

896 Mahowald, N. M., Hamilton, D. S., Mackey, K. R. M., Moore, J. K., Baker, A. R., Scanza, R.
897 A., and Zhang, Y.: Aerosol trace metal leaching and impacts on marine microorganisms, Nature
898 Communications, 9, 2614, https://doi.org/10.1038/s41467-018-04970-7, 2018.

899 Mao, J., Fan, S., and Horowitz, L. W.: Soluble Fe in Aerosols Sustained by Gaseous HO2
900 Uptake, Environmental Science & Technology Letters, 4, 98-104,
901 https://doi.org/10.1021/acs.estlett.7b00017, 2017.

902 Mao, J., Fan, S., Jacob, D. J., and Travis, K. R.: Radical loss in the atmosphere from Cu-Fe
903 redox coupling in aerosols, Atmos. Chem. Phys., 13, 509-519, 10.5194/acp-13-509-2013, 2013.

904 Nriagu, J. O.: A global assessment of natural sources of atmospheric trace metals, Nature, 338,
905 47-49, https://doi.org/10.1038/338047a0, 1989.

906 Oakes, M., Ingall, E. D., Lai, B., Shafer, M. M., Hays, M. D., Liu, Z. G., Russell, A. G., and
907 Weber, R. J.: Iron Solubility Related to Particle Sulfur Content in Source Emission and Ambient
908 Fine Particles, Environmental Science & Technology, 46, 6637-6644,
909 https://doi.org/10.1021/es300701c, 2012.

910 Paatero, P.: Least squares formulation of robust non-negative factor analysis, Chemometrics
911 and Intelligent Laboratory Systems, 37, 23-35, https://doi.org/10.1016/S0169-7439(96)00044-
912 5, 1997.

913 Paatero, P. and Tapper, U.: Positive matrix factorization: A non-negative factor model with

914 optimal utilization of error estimates of data values, Environmetrics, 5, 111-126,
915 https://doi.org/10.1002/env.3170050203, 1994.

916 Paris, R. and Desboeufs, K. V.: Effect of atmospheric organic complexation on iron-bearing
917 dust solubility, Atmospheric Chemistry and Physics, 13, 4895-4905,
918 https://doi.org/10.5194/acp-13-4895-2013, 2013.

919 Paris, R., Desboeufs, K. V., and Journet, E.: Variability of dust iron solubility in atmospheric
920 waters: Investigation of the role of oxalate organic complexation, Atmospheric Environment,
921 45, 6510-6517, https://doi.org/10.1016/j.atmosenv.2011.08.068, 2011.

922 Paytan, A., Mackey, K. R. M., Chen, Y., Lima, I. D., Doney, S. C., Mahowald, N., Labiosa, R.,
923 and Postf, A. F.: Toxicity of atmospheric aerosols on marine phytoplankton, Proceedings of the
924 National Academy of Sciences of the United States of America, 106, 4601-4605,
925 https://doi.org/10.1073/pnas.0811486106, 2009.

926 Phalen, R. F.: The particulate air pollution controversy, Nonlinearity Biol Toxicol Med, 2, 259-
927 292, https://doi.org/10.1080/15401420490900245, 2004.

928 Pye, H. O. T., Nenes, A., Alexander, B., Ault, A. P., Barth, M. C., Clegg, S. L., Collett Jr, J. L.,
929 Fahey, K. M., Hennigan, C. J., Herrmann, H., Kanakidou, M., Kelly, J. T., Ku, I. T., McNeill,
930 V. F., Riemer, N., Schaefer, T., Shi, G., Tilgner, A., Walker, J. T., Wang, T., Weber, R., Xing, J.,
931 Zaveri, R. A., and Zuend, A.: The acidity of atmospheric particles and clouds, Atmos. Chem.
932 Phys., 20, 4809-4888, https://doi.org/10.5194/acp-20-4809-2020, 2020.

933 Schroth, A. W., Crusius, J., Sholkovitz, E. R., and Bostick, B. C.: Iron solubility driven by
934 speciation in dust sources to the ocean, Nature Geoscience, 2, 337-340,
935 https://doi.org/10.1038/ngeo501, 2009.

936 Sedwick, P. N., Sholkovitz, E. R., and Church, T. M.: Impact of anthropogenic combustion
937 emissions on the fractional solubility of aerosol iron: Evidence from the Sargasso Sea,
938 Geochemistry, Geophysics, Geosystems, 8, https://doi.org/10.1029/2007GC001586, 2007.

939 Shelley, R. U., Landing, W. M., Ussher, S. J., Planquette, H., and Sarthou, G.: Regional trends
940 in the fractional solubility of Fe and other metals from North Atlantic aerosols (GEOTRACES
941 cruises GA01 and GA03) following a two-stage leach, Biogeosciences, 15, 2271-2288,
942 https://doi.org/10.5194/bg-15-2271-2018, 2018.

943 Shi, J., Guan, Y., Ito, A., Gao, H., Yao, X., Baker, A. R., and Zhang, D.: High Production of
944 Soluble Iron Promoted by Aerosol Acidification in Fog, Geophysical Research Letters, 47,
945 e2019GL086124, https://doi.org/10.1029/2019GL086124, 2020.

946 Sholkovitz, E. R., Sedwick, P. N., Church, T. M., Baker, A. R., and Powell, C. F.: Fractional
947 solubility of aerosol iron: Synthesis of a global-scale data set, Geochimica et Cosmochimica
948 Acta, 89, 173-189, https://doi.org/10.1016/j.gca.2012.04.022, 2012.

949 Slikboer, S., Grandy, L., Blair, S. L., Nizkorodov, S. A., Smith, R. W., and Al-Abadleh, H. A.:

Formation of Light Absorbing Soluble Secondary Organics and Insoluble Polymeric Particles from the Dark Reaction of Catechol and Guaiacol with Fe(III), Environmental Science & Technology, 49, 7793-7801, https://doi.org/10.1021/acs.est.5b01032, 2015.

Spokes, L. J., Jickells, T. D., and Lim, B.: Solubilisation of aerosol trace metals by cloud processing: A laboratory study, Geochimica et Cosmochimica Acta, 58, 3281-3287, https://doi.org/10.1016/0016-7037(94)90056-6, 1994.

Tao, Y. and Murphy, J. G.: The Mechanisms Responsible for the Interactions among Oxalate, pH, and Fe Dissolution in PM2.5, ACS Earth and Space Chemistry, 3, 2259-2265, https://doi.org/10.1021/acsearthspacechem.9b00172, 2019.

Wang, W., Liu, M., Wang, T., Song, Y., Zhou, L., Cao, J., Hu, J., Tang, G., Chen, Z., Li, Z., Xu, Z., Peng, C., Lian, C., Chen, Y., Pan, Y., Zhang, Y., Sun, Y., Li, W., Zhu, T., Tian, H., and Ge, M.: Sulfate formation is dominated by manganese-catalyzed oxidation of SO2 on aerosol surfaces during haze events, Nature Communications, 12, https://doi.org/10.1038/s41467-021-22091-6, 2021.

Wang, Z. Z., Fu, H. B., Zhang, L. W., Song, W. H., and Chen, J. M.: Ligand-Promoted Photoreductive Dissolution of Goethite by Atmospheric Low-Molecular Dicarboxylates, Journal of Physical Chemistry A, 121, 1648-1657, https://doi.org/10.1021/acs.jpca.6b09160, 2017.

Wong, J. P. S., Yang, Y., Fang, T., Mulholland, J. A., Russell, A. G., Ebelt, S., Nenes, A., and Weber, R. J.: Fine Particle Iron in Soils and Road Dust Is Modulated by Coal-Fired Power Plant Sulfur, Environmental Science & Technology, 54, 7088-7096, https://doi.org/10.1021/acs.est.0c00483, 2020.

Ye, D., Klein, M., Mulholland, J. A., Russell, A. G., Weber, R., Edgerton, E. S., Chang, H. H., Sarnat, J. A., Tolbert, P. E., and Ebelt Sarnat, S.: Estimating Acute Cardiovascular Effects of Ambient PM2.5 Metals, Environmental Health Perspectives, 126, 027007, https://doi.org/10.1289/ehp2182, 2018.

Zhang, H., Li, R., Dong, S., Wang, F., Zhu, Y., Meng, H., Huang, C., Ren, Y., Wang, X., Hu, X., Li, T., Peng, C., Zhang, G., Xue, L., Wang, X., and Tang, M.: Abundance and Fractional Solubility of Aerosol Iron During Winter at a Coastal City in Northern China: Similarities and Contrasts Between Fine and Coarse Particles, Journal of Geophysical Research: Atmospheres, 127, e2021JD036070, https://doi.org/10.1029/2021JD036070, 2022.

Zhao, Z., Luo, X. S., Jing, Y. S., Li, H. B., Pang, Y. T., Wu, L. C., Chen, Q., and Jin, L.: In vitro assessments of bioaccessibility and bioavailability of PM2.5 trace metals in respiratory and digestive systems and their oxidative potential, Journal of Hazardous Materials, 409, https://doi.org/10.1016/j.jhazmat.2020.124638, 2021.

Zhong, L., Louie, P. K. K., Zheng, J., Yuan, Z., Yue, D., Ho, J. W. K., and Lau, A. K. H.: Science–policy interplay: Air quality management in the Pearl River Delta region and Hong

Kong, Atmospheric Environment, 76, 3-10, https://doi.org/10.1016/j.atmosenv.2013.03.012, 2013.

Zhou, Y., Zhang, Y., Griffith, S. M., Wu, G., Li, L., Zhao, Y., Li, M., Zhou, Z., and Yu, J. Z.: Field Evidence of Fe-Mediated Photochemical Degradation of Oxalate and Subsequent Sulfate Formation Observed by Single Particle Mass Spectrometry, Environmental Science & Technology, 54, 6562-6574, https://doi.org/10.1021/acs.est.0c00443, 2020.

Zhu, X., Prospero, J. M., Savoie, D. L., Millero, F. J., Zika, R. G., and Saltzman, E. S.: Photoreduction of iron(III) in marine mineral aerosol solutions, Journal of Geophysical Research: Atmospheres, 98, 9039-9046, https://doi.org/10.1029/93JD00202, 1993.

Zhu, Y., Li, W., Lin, Q., Yuan, Q., Liu, L., Zhang, J., Zhang, Y., Shao, L., Niu, H., Yang, S., and Shi, Z.: Iron solubility in fine particles associated with secondary acidic aerosols in east China, Environmental Pollution, 264, 114769, https://doi.org/10.1016/j.envpol.2020.114769, 2020.

Measurement Report: Abundance and fractional solubilities of aerosol metals in urban Hong Kong: Insights into factors that control aerosol metal dissolution in an urban site in South China

Junwei Yang,[1] Lan Ma,[1] Xiao He,[2] Wing Chi Au,[1] Yanhao Miao,[1] Wen-Xiong Wang,[1,3] Theodora Nah[1,3]*

[1]*School of Energy and Environment, City University of Hong Kong, Hong Kong SAR, China*

[2]*College of Chemistry and Environmental Engineering, Shenzhen University, Shenzhen 518060, China*

[3]*State Key Laboratory of Marine Pollution, City University of Hong Kong, Hong Kong SAR, China*

** To whom correspondence should be addressed: Theodora Nah (Email: theodora.nah@cityu.edu.hk)*

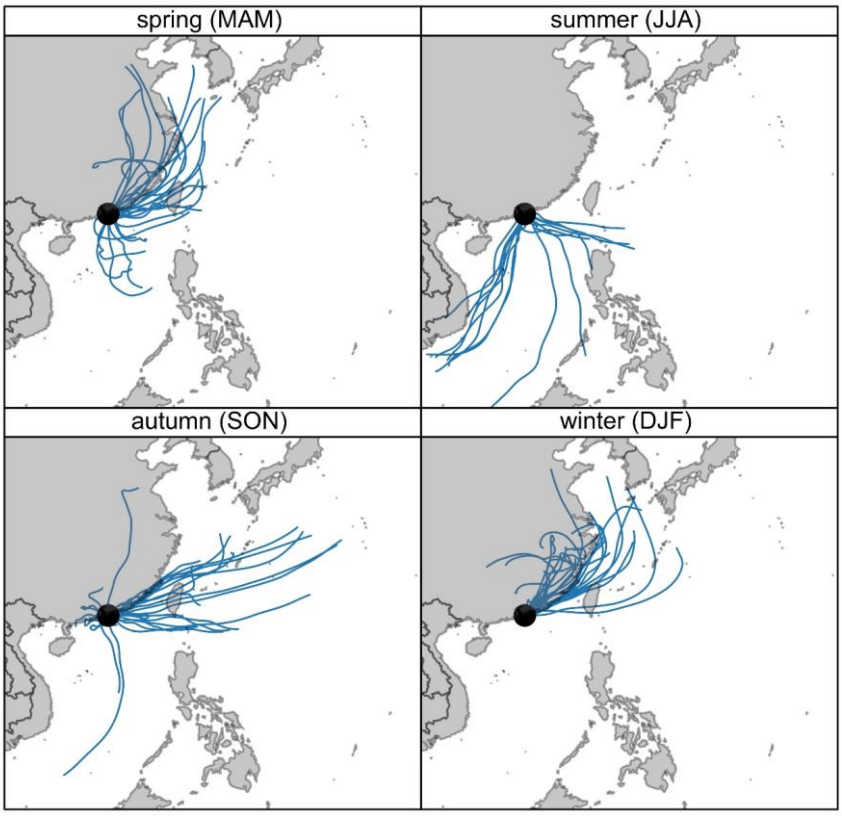

Figure S1: Back trajectories of air masses reaching Hong Kong (latitude = 22.303, longitude = 114.177, height = 100 m, duration = 72 h) during the four sampling periods. Back-trajectories calculations were performed by the Hybrid Split-Particle Lagrangian Integrated Trajectory (HYSPLIT) model using meteorological data from NCEP/NCAR Reanalysis (2.5° latitude-longitude grid).

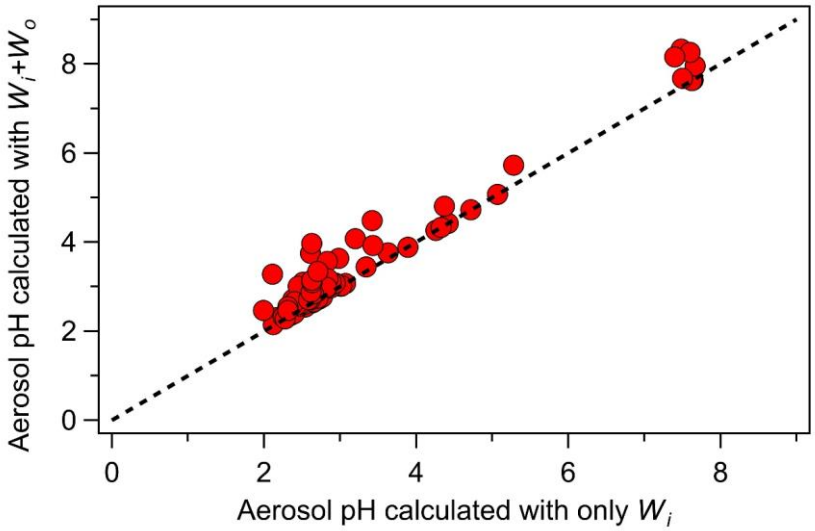

Figure S2: Comparisons of aerosol pH values calculated with (y axis) vs. without (x axis) contributions from W_o. The dashed line is the 1:1 line. Majority of the predicted pH values lie close to the dashed line. This indicated that the inclusion/exclusion of W_o into calculations did not impact aerosol pH significantly.

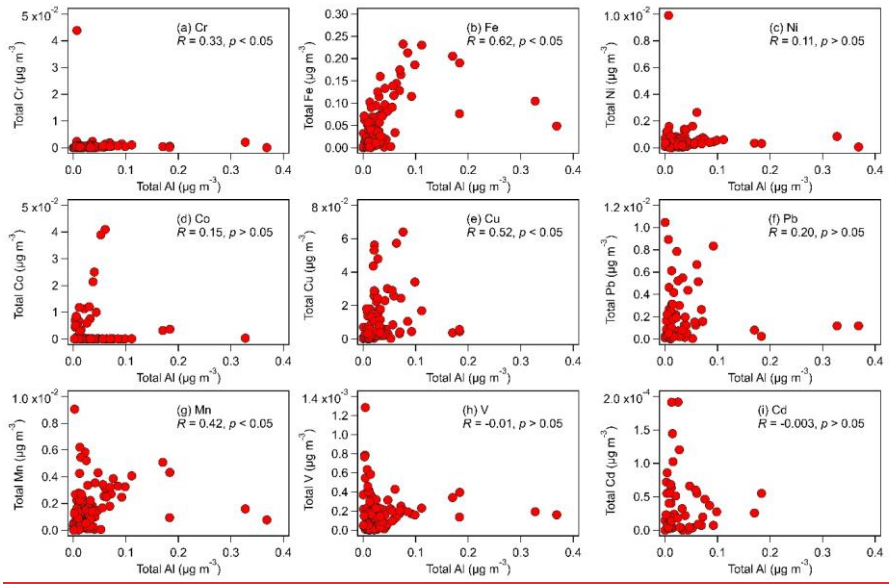

Figure S3: Relationships between the mass concentrations of total Al and the other total metals in coarse and fine aerosols. Only data with non-zero total metal concentrations were used in the figures. Also shown are the spearman correlation coefficients for each relationship.

Formatted: Indent: Left 0 ch

Deleted: for both

Formatted: Justified

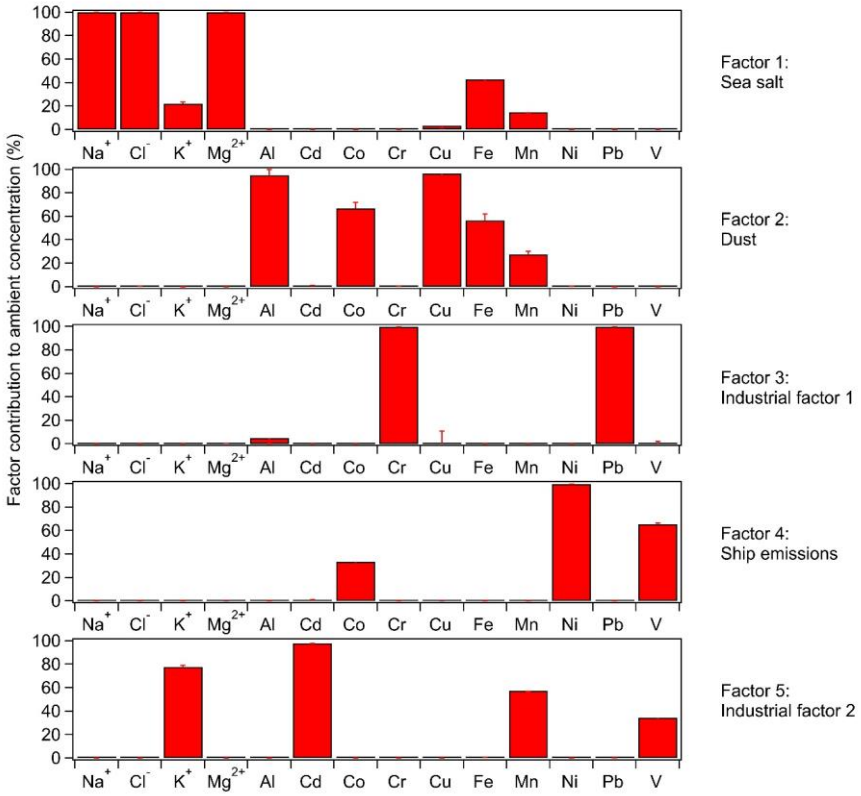

Figure S4: Profiles of the five factors resolved by positive matrix factorization (PMF) using bootstrap (BS) analysis for source apportionment of aerosols measured at the monitoring site. The error bars represent the largest displacement (DISP) uncertainty range from the base run.

Formatted: Don't add space between paragraphs of the same style

Deleted: S3

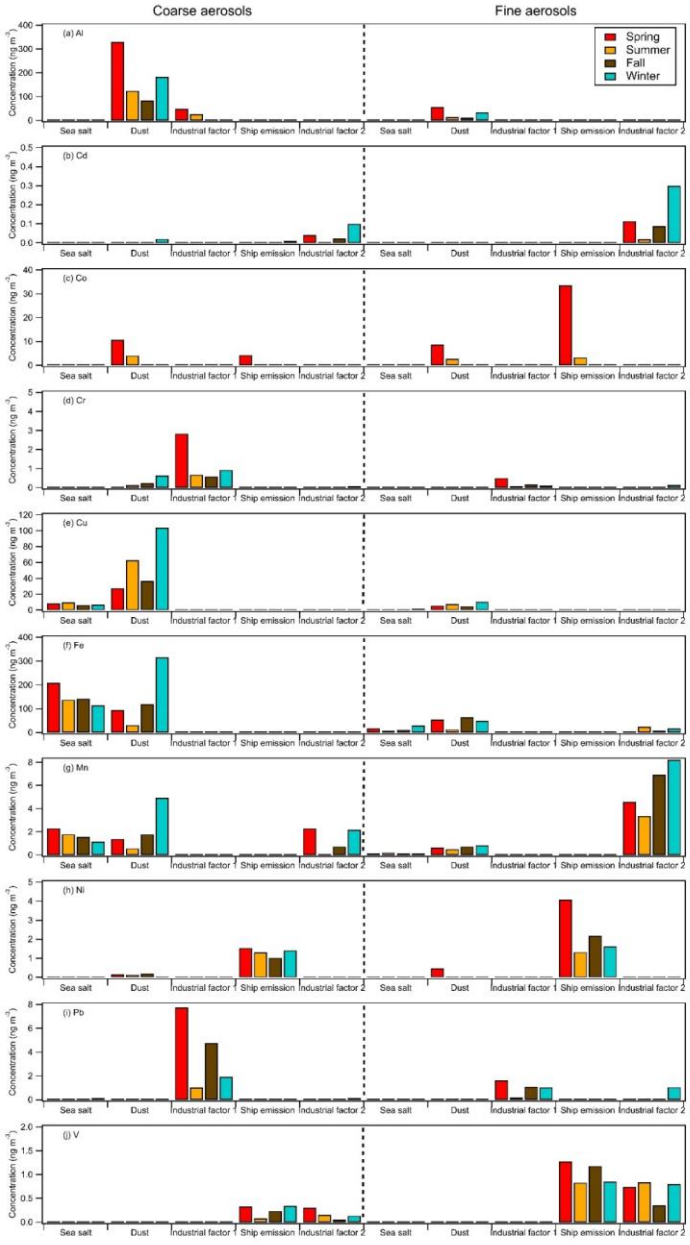

38

39 **Figure S5:** Seasonal mass contributions of each source to each species in coarse and fine

40 aerosols.

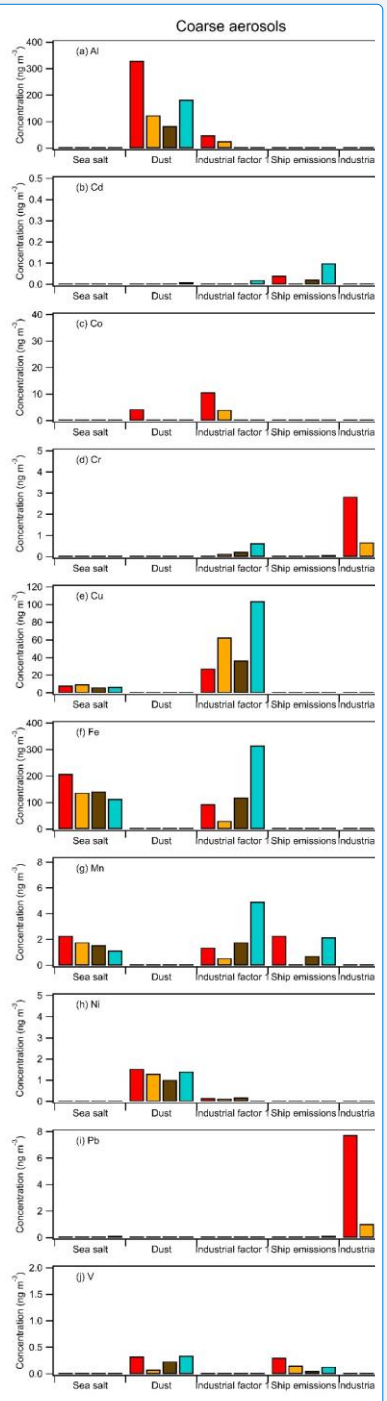

Deleted:

Formatted: Don't add space between paragraphs of the same style

Deleted: S4

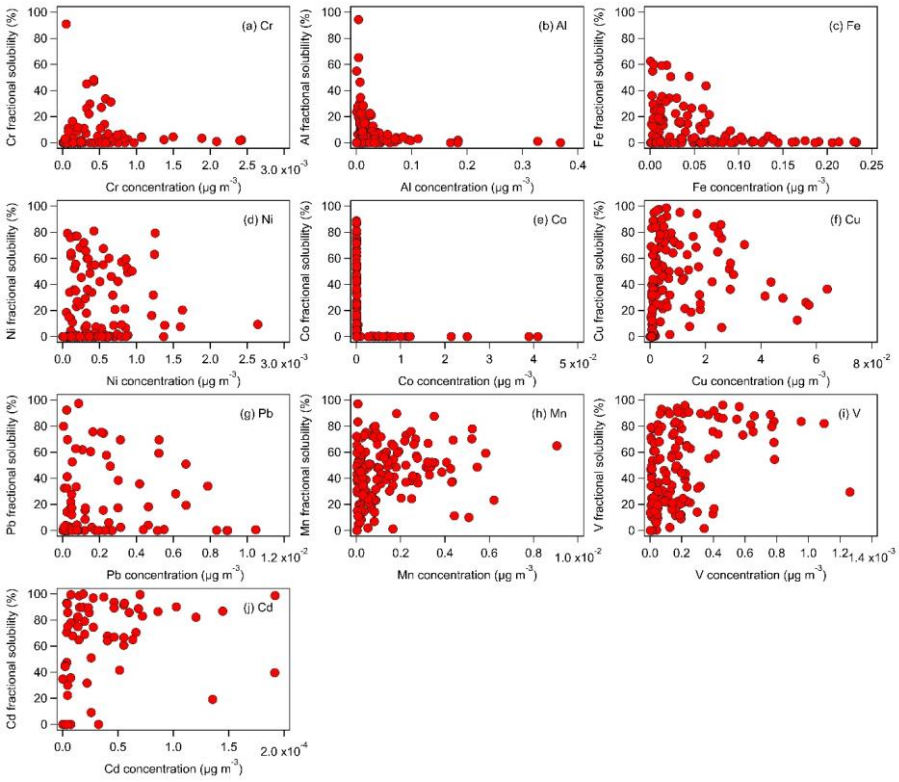

Figure S6: Metal fractional solubility vs. total metal concentration for fine and coarse aerosols. The fractional solubility values were calculated by dividing the water-soluble metal mass concentration by the total metal mass concentration. Only data with non-zero total metal concentrations were used in the figures.

Deleted: S5

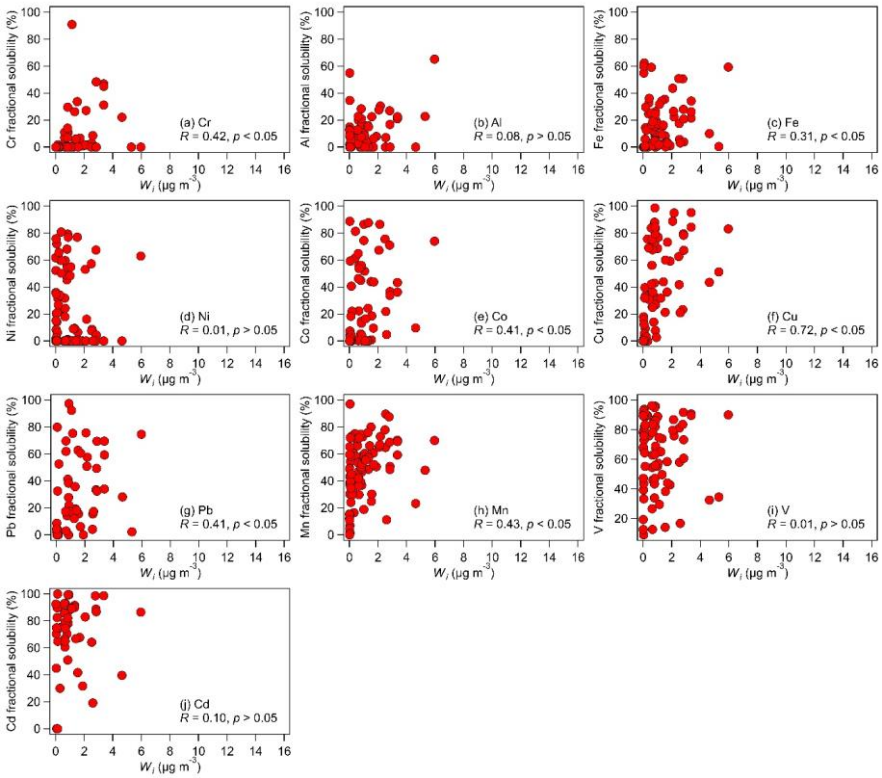

Figure S7: Relationships between the metal fractional solubilities and W_i in fine aerosols. Only data with non-zero total metal concentrations were used in the figures. Also shown are the spearman correlation coefficients for each relationship.

Deleted: S6

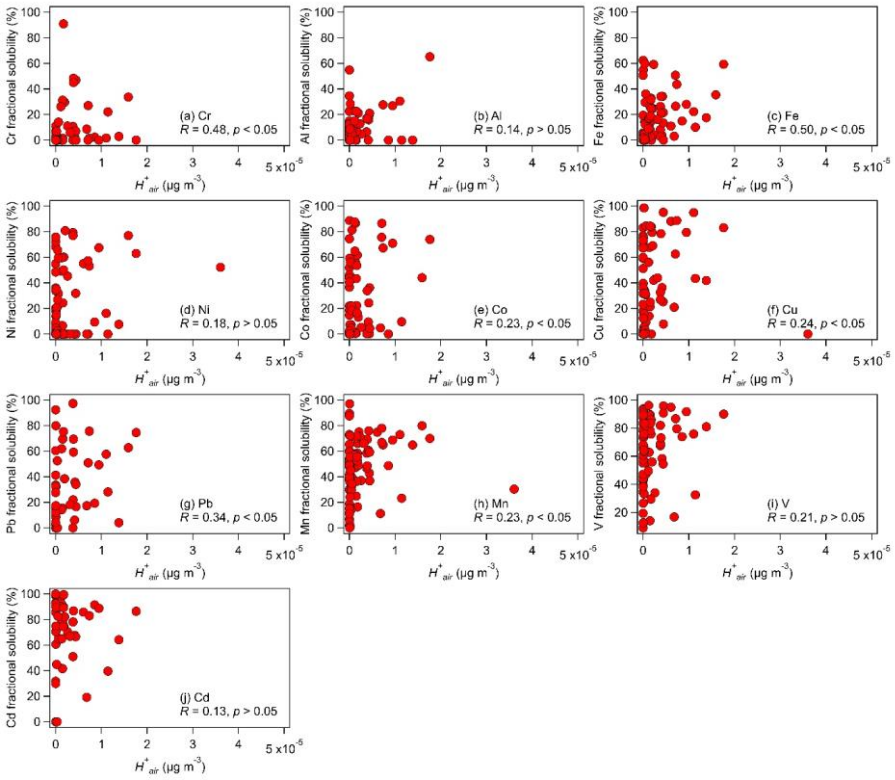

Figure S8: Relationships between the metal fractional solubilities and H^+_{air} in fine aerosols. Only data with non-zero total metal concentrations were used in the figures. Also shown are the spearman correlation coefficients for each relationship.

Deleted: S7

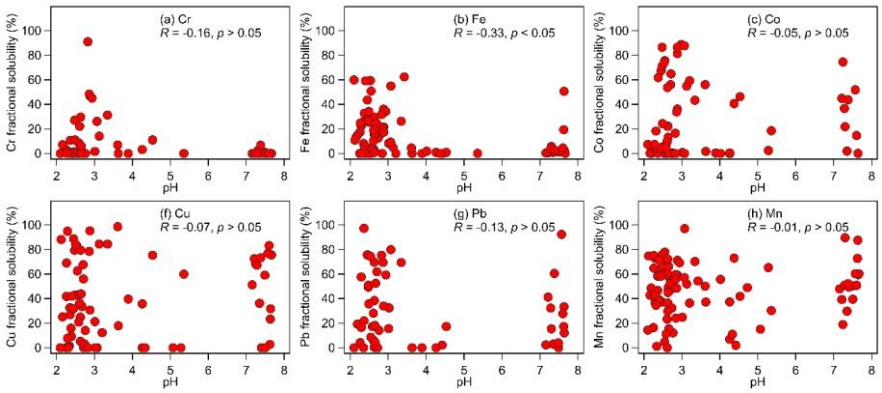

Figure S9: Relationships between the Cr, Fe, Co, Cu, Pb, and Mn fractional solubilities and fine aerosol pH. Only data with non-zero total metal concentrations were used in the figures. Also shown are the spearman correlation coefficients for each relationship. Only the correlation between the Fe fractional solubility and fine aerosol pH was statistically significant.

Deleted: S8

Table S1: Comparison of average total metal concentrations (ng m^{-3}) in 2012/2013 by Jiang et al. (2015) and 2021/2022 (this study) at a Kowloon Tong in Hong Kong

(a) Comparison of winter mass concentrations

Metal	Jiang et al. (2015)[a]		This study[b]	
	Fine	Coarse[c]	Fine	Coarse[c]
Cr	3	2.7	1.11	0.94
Al	254	301.2	78.53	135.12
Fe	137	142	204.71	301.22
Ni	4.4	1.6	1.97	0.84
Cu	19.7	4	20.61	61.20
Pb	49.4	2.9	8.98	0.86
Mn	17.1	5.2	11.82	5.18
V	9.2	0.9	1.41	0.30
Cd	1.1	0.1	0.22	0.03

[a] Measurements were performed from 12 November 2012 to 10 December 2012.
[b] Measurements were performed from 15 December 2021 to 26 January 2022.
[c] Mass concentrations measured for the MOUDI impactor stage 11 (18 µm nominal cutoff) was excluded in this comparison since Jiang et al. (2015) reported mass concentrations for $PM_{2.5-10}$ for their coarse aerosol measurements.

(b) Comparison of spring/summer mass concentrations

Metal	Jiang et al. (2015)[a]		This study[b]	
	Fine	Coarse[c]	Fine	Coarse[c]
Cr	7.2	1.5	2.53	1.24
Al	591	528.9	107.14	237.76
Fe	190.6	153	150.33	163.59
Ni	10	1.3	3.84	0.94
Cu	21.6	5.5	11.98	24.16
Pb	52.7	2.8	6.92	3.69
Mn	19.3	5	6.45	2.87
V	25.6	1.8	1.90	0.31
Cd	1.2	0.1	0.08	0.01

[a] Measurements were performed from 8 April 2013 to 13 May 2013.
[b] Measurements were performed from 7 March 2021 to 4 April 2021, 23 to 30 June 2021, and 7 to 14 July 2021.
[c] Mass concentrations measured for the MOUDI impactor stage 11 (18 µm nominal cutoff) was excluded in this comparison since Jiang et al. (2015) reported mass concentrations for $PM_{2.5-10}$ for their coarse aerosol measurements.

Deleted: 0.68
Deleted: 1.66
Formatted ...
Formatted ...
Deleted: 47.54
Deleted: 184.67
Formatted ...
Formatted ...
Deleted: 95.70
Deleted: 432.04
Formatted ...
Formatted ...
Deleted: 1.63
Deleted: 1.43
Formatted ...
Formatted ...
Deleted: 10.06
Formatted ...
Formatted ...
Deleted: 106.92
Deleted: 8.52
Deleted: 2.06
Formatted ...
Formatted ...
Deleted: 9.20
Deleted: 8.25
Formatted ...
Formatted ...
Deleted: 1.25
Deleted: 0.48
Formatted ...
Formatted ...
Deleted: 0.18
Deleted: 0.06
Formatted ...
Formatted ...
Formatted ...
Deleted: 1.86
Deleted: 2.15
Formatted ...
Deleted: 60.47
Deleted: 302.70
Formatted ...
Formatted ...
Formatted ...
Formatted ...
Formatted ...

Table S2: Spearman rank correlations between the water-soluble and total metals in fine and coarse aerosols[a]

Metal	Fine	Coarse
Cr	**0.49**	**0.50**
Al	**0.40**	0.14
Fe	**0.58**	**0.48**
Ni	**0.43**	**0.30**
Co	0.16	0.06
Cu	**0.86**	**0.81**
Pb	**0.60**	**0.43**
Mn	**0.93**	**0.95**
V	**0.89**	**0.81**
Cd	**0.96**	**0.64**

[a] Bold: statistically significant ($p < 0.05$)

Table S3: Spearman rank correlations between the metal fractional solubilities and nitrate and aerosol properties[a]

Metal	Nitrate	Ammonium	RH	Temp
Cr	**0.67**	**0.51**	**-0.53**	**-0.78**
Al	-0.05	0.09	-0.07	-0.09
Fe	-0.04	**0.39**	0.01	0.06
Ni	**-0.26**	-0.05	**0.25**	**0.77**
Co	0.16	**0.33**	-0.01	0.02
Cu	**0.67**	**0.59**	0.00	0.00
Pb	**0.34**	**0.38**	-0.25	-0.12
Mn	0.14	**0.22**	0.02	-0.11
V	**-0.29**	**0.23**	0.18	0.10
Cd	-0.16	0.11	0.08	-0.17

[a] Bold: statistically significant ($p < 0.05$)

Deleted: ¶
Metal

Section S1. Source apportionment

To identify the major sources of the measured total aerosol metals, source apportionment was performed with positive matrix factorization (PMF) using EPA PMF 5.0 software. PMF decomposes the measured concentration matrix (x_{ij}) into two matrices: the factor contributions matrix (g_{ik}) and factor profiles (f_{kj}) plus a residue matrix (e_{ij}) (Paatero and Tapper, 1994; Paatero, 1997):

$$x_{ij} = \sum_{k=1}^{p} g_{ik} f_{kj} + e_{ij} \cdots \quad (1)$$

where p is the number of factors determined by the user. Factor contributions and profiles are determined by minimizing the objective function (Q):

$$\mathrm{Q} = \sum_{i=1}^{n} \sum_{j=1}^{m} \left[\frac{x_{ij} - \sum_{k=1}^{p} g_{ik} f_{kj}}{u_{ij}} \right]^2 \cdots \quad (2)$$

where u_{ij} is the uncertainty matrix provide by the user. The ultimate goal is to achieve chemical mass balance between the measured species and source contributions by minimizing Q. Two error estimation approaches were used to analyze the model-resolved factor profiles: Bootstrap (BS) and Displacement (DISP) (Paatero et al., 2014). The EPA PMF 5.0 software conducts BS by randomly perturbing the original data set and generating new PMF results using the resampled version of input data. The BS factor is subsequently assigned to the base run factor with which the BS factor has the highest correlation, above a user-defined threshold. BS estimation involves uncertainties derived from random errors and partially from rotational ambiguity. The EPA PMF 5.0 software performs DISP by "displacing" each variable in the well-fitted factor f_{kj} far enough such that Q increases by a pre-defined maximum value dQ^{max}. Such extensions estimate the upper and lower intervals of each species in the factor profile. By nature, DISP reflects the uncertainty derived from rotational ambiguity.

The mass concentrations of 14 chemical species (Na^+, Cl^-, K^+, Mg^{2+}, ^{27}Al, ^{51}V, ^{52}Cr, ^{55}Mn, ^{57}Fe, ^{59}Co, ^{60}Ni, ^{65}Cu, ^{111}Cd, and ^{208}Pb) measured on each MOUDI stage during every sampling period (total of 175 sets of samples) were used as the input matrix. 100 BS runs were performed. Uncertainties were as following:

$$u_{ij} = \sqrt{(x_{ij} \times EF)^2 + (MDL)^2} \cdots \quad (3)$$

where x_{ij} is the measured concentration, EF is the user-defined error fraction for individual species derived from the experimental data, and MDL is the method detection limit. For concentrations below MDL, the uncertainty was set to 5/6 × MDL. In PMF, the optimal number of factors is a compromise between resolving factors with the best physical meanings and a good fit for all input species. 3 to 7 factors were tested, and the final number was determined by examining the changes in Q_{robust}/Q_{exp} and the physical interpretation of each factor. $Q_{exp} \approx nm - p(n+m)$, denotes the degree of freedom of the model solution, where n, m, and p refer to the number of samples, the number of species input into PMF, and the number of factors. Based on the minimal Q values and the physical interpretations of the resolved factor, the five-factor solution was selected. These five factors were broadly classified as: Sea salt, Dust, Industrial, Residual oil, and Ship emissions. The Q_{robust}/Q_{exp} changed 14.8% from a four-factor to a five-factor solution, while the Q_{robust}/Q_{exp} changed 22.6% from a three-factor solution to a four-factor solution.

Figure S3 shows the factor profiles resolved in the five-factor solution. Source identification was based on the tracer species with the highest mass loadings. The first factor was marked by the high loadings of common sea salt tracers Na^+, Cl^-, and Mg^{2+}, thus it was identified as "sea salt" (Chow et al., 2022). Interestingly, the "sea salt" factor had a noticeably high Fe loading. Previous studies have reported Fe deposition to marine waters from continental outflows of mineral dust, biomass burning aerosols, and oil fly ash (Ito, 2013; Wang et al., 2015; Matsui et al., 2018). This could result in substantial concentrations of Fe in sea salt, which in turn would lead to the high loading of Fe in the "sea salt" factor. The second factor was identified as "dust" due to its high loadings of Al, Fe, and Mn, which are known mineral dust tracers (Chow et al., 2022). Cu is also a dominant species in this second factor. Previous studies have attributed Cu to brake/tire wear, and Fe and Mn to both dust and brake/tire wear (Garg et al., 2000; Adachi and Tainosho, 2004; Lough et al., 2005). Thus, resuspended road dust containing brake/tire wear particles could have contributed to this "dust" factor. Interestingly, the "dust" factor had a noticeably high Co loading. This could be explained by Co being widely found in rocks, soil, water, and plants. It is the 33rd abundant elements in

Deleted: Fe has been reported to

Deleted: concentration of Fe in sea salt, which led to the high loading of Fe in the "sea salt" factor

Earth's crust with an average concentration of 20 µg/g (Lison, 1996). While Co can also be emitted from anthropogenic sources such as coal-fired power generation, vehicle exhaust, and mining activities (Wu et al., 2022; Johansson et al., 2009), these sources were not resolved in this work since we did not measure their source-specific tracers. The fourth factor was identified as "ship emissions" since it was marked by high loadings of Ni and V, which are known tracers for ship emissions (Chow et al., 2022). The third and fifth factors were broadly classified as "industrial factor 1" and "industrial factor 2" since their dominant metal species are typically associated with industrial emissions (Chow et al., 2022).

Section S2. Aerosol liquid water concentration associated with organics

The following equation was used to calculated the aerosol liquid water concentration (µg m^{-3}) associated with organic species (Guo et al., 2015):

$$W_o = \frac{m_{org}\rho_w}{\rho_{org}} \frac{\kappa_{org}}{(\frac{1}{RH}-1)} \quad (4)$$

where m_{org} is the organic mass concentration (µg m^{-3}), ρ_w is the water density (1 µg m^{-3}), ρ_{org} is the organic density, k_{org} is the organic hygroscopicity parameter, and RH is the relative humidity of the sampling period. We calculated m_{org} by multiplying the measured water-soluble organic carbon (WSOC) concentration by 1.6, which is the conversion factor recommended for converting WSOC to organic mass in urban aerosols (Turpin and Lim, 2001). We assumed ρ_{org} to be 1.4 g cm^{-3}, which is the value usually assumed for the density of ambient organic aerosols in previous studies (Guo et al., 2015; Shiraiwa et al., 2017; Kuwata et al., 2012; King et al., 2007). We used 0.35 for κ_{org}, which is the average of the range of values (0.28 to 0.39) previously measured for organic aerosols in Hong Kong (Meng et al., 2014).

References

Adachi, K. and Tainosho, Y.: Characterization of heavy metal particles embedded in tire dust,

Environment International, 30, 1009-1017, https://doi.org/10.1016/j.envint.2004.04.004, 2004.

Chow, W. S., Huang, X. H. H., Leung, K. F., Huang, L., Wu, X., and Yu, J. Z.: Molecular and elemental marker-based source apportionment of fine particulate matter at six sites in Hong Kong, China, Science of The Total Environment, 813, 152652, https://doi.org/10.1016/j.scitotenv.2021.152652, 2022.

Garg, B. D., Cadle, S. H., Mulawa, P. A., Groblicki, P. J., Laroo, C., and Parr, G. A.: Brake Wear Particulate Matter Emissions, Environmental Science & Technology, 34, 4463-4469, 10.1021/es001108h, 2000.

Guo, H., Xu, L., Bougiatioti, A., Cerully, K. M., Capps, S. L., Hite Jr, J. R., Carlton, A. G., Lee, S. H., Bergin, M. H., Ng, N. L., Nenes, A., and Weber, R. J.: Fine-particle water and pH in the southeastern United States, Atmos. Chem. Phys., 15, 5211-5228, 10.5194/acp-15-5211-2015, 2015.

Ito, A.: Global modeling study of potentially bioavailable iron input from shipboard aerosol sources to the ocean, Global Biogeochemical Cycles, 27, 1-10, https://doi.org/10.1029/2012GB004378, 2013.

Jiang, S. Y., Kaul, D. S., Yang, F., Sun, L., and Ning, Z.: Source apportionment and water solubility of metals in size segregated particles in urban environments, Science of The Total Environment, 533, 347-355, https://doi.org/10.1016/j.scitotenv.2015.06.146, 2015.

Johansson, C., Norman, M., and Burman, L.: Road traffic emission factors for heavy metals, Atmospheric Environment, 43, 4681-4688, https://doi.org/10.1016/j.atmosenv.2008.10.024, 2009.

King, S. M., Rosenoern, T., Shilling, J. E., Chen, Q., and Martin, S. T.: Cloud condensation nucleus activity of secondary organic aerosol particles mixed with sulfate, Geophysical Research Letters, 34, https://doi.org/10.1029/2007GL030390, 2007.

Kuwata, M., Zorn, S. R., and Martin, S. T.: Using elemental ratios to predict the density of organic material composed of carbon, hydrogen, and oxygen, Environ Sci Technol, 46, 787-794, https://doi.org/10.1021/es202525q, 2012.

Lison, D.: Human Toxicity of Cobalt-Containing Dust and Experimental Studies on the Mechanism of Interstitial Lung Disease (Hard Metal Disease), Critical Reviews in Toxicology, 26, 585-616, 10.3109/10408449609037478, 1996.

Lough, G. C., Schauer, J. J., Park, J.-S., Shafer, M. M., DeMinter, J. T., and Weinstein, J. P.: Emissions of Metals Associated with Motor Vehicle Roadways, Environmental Science & Technology, 39, 826-836, 10.1021/es048715f, 2005.

Matsui, H., Mahowald, N. M., Moteki, N., Hamilton, D. S., Ohata, S., Yoshida, A., Koike, M., Scanza, R. A., and Flanner, M. G.: Anthropogenic combustion iron as a complex climate forcer, Nature Communications, 9, 1593, 10.1038/s41467-018-03997-0, 2018.

Meng, J. W., Yeung, M. C., Li, Y. J., Lee, B. Y. L., and Chan, C. K.: Size-resolved cloud condensation nuclei (CCN) activity and closure analysis at the HKUST Supersite in Hong Kong, Atmos. Chem. Phys., 14, 10267-10282, 10.5194/acp-14-10267-2014, 2014.

Paatero, P.: Least squares formulation of robust non-negative factor analysis, Chemometrics and Intelligent Laboratory Systems, 37, 23-35, https://doi.org/10.1016/S0169-7439(96)00044-5, 1997.

Paatero, P. and Tapper, U.: Positive matrix factorization: A non-negative factor model with optimal utilization of error estimates of data values, Environmetrics, 5, 111-126, https://doi.org/10.1002/env.3170050203, 1994.

Paatero, P., Eberly, S., Brown, S. G., and Norris, G. A.: Methods for estimating uncertainty in factor analytic solutions, Atmos Meas Tech, 7, 781-797, 10.5194/amt-7-781-2014, 2014.

Shiraiwa, M., Li, Y., Tsimpidi, A. P., Karydis, V. A., Berkemeier, T., Pandis, S. N., Lelieveld, J., Koop, T., and Pöschl, U.: Global distribution of particle phase state in atmospheric secondary organic aerosols, Nature Communications, 8, 15002, https://doi.org/10.1038/ncomms15002, 2017.

Turpin, B. J. and Lim, H.-J.: Species Contributions to PM2.5 Mass Concentrations: Revisiting Common Assumptions for Estimating Organic Mass, Aerosol Science and Technology, 35, 602-610, https://doi.org/10.1080/02786820119445, 2001.

Wang, R., Balkanski, Y., Boucher, O., Bopp, L., Chappell, A., Ciais, P., Hauglustaine, D., Peñuelas, J., and Tao, S.: Sources, transport and deposition of iron in the global atmosphere, Atmos. Chem. Phys., 15, 6247-6270, 10.5194/acp-15-6247-2015, 2015.

Wu, Y., Liu, Q., Ma, J., Zhao, W., Chen, H., and Qu, Y.: Antimony, beryllium, cobalt, and vanadium in urban park soils in Beijing: Machine learning-based source identification and health risk-based soil environmental criteria, Environmental Pollution, 293, 118554, https://doi.org/10.1016/j.envpol.2021.118554, 2022.